In presenting the dissertation as a partial fulfillment of the requirements for an advanced degree from the Georgia Institute of Technology, I agree that the Library of the Institute shall make it available for inspection and circulation in accordance with its regulations governing materials of this type. I agree that permission to copy from, or to publish from, this dissertation may be granted by the professor under whose direction it was written, or, in his absence, by the Dean of the Graduate Division when such copying or publication is solely for scholarly purposes and does not involve potential financial gain. It is understood that any copying from, or publication of, this dissertation which involves potential financial gain will not be allowed without written permission.

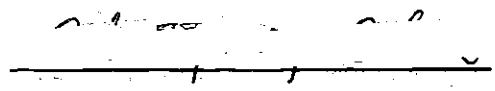

7/25/68

REMOVAL OF A SPHERICAL PARTICLE FROM A FLAT BED

A THESIS

Presented to

The Faculty of the Division of Graduate

Studies and Research

by

Charng Ning Chen

In Partial Fulfillment

of the Requirements for the Degree

Doctor of Philosophy

in the School of Civil Engineering

Georgia Institute of Technology

October, 1970

REMOVAL OF A SPHERICAL PARTICLE

FROM A FLAT BED

Approved:

Chairman

Date approved by Chairman: 12/1/70

Dedicated to

my mother,

Chien-Wu Lin Chen

ACKNOWLEDGMENTS

The author would like to express his sincere thanks to Professor M. R. Carstens for his expert guidance during the course of the present study. Dr. Carstens initiated the present investigation and offered many valuable suggestions.

To Dr. W. M. Sangster, Director of the School of Civil Engineering, and Dr. C. W. Gorton, Professor of the School of Chemical Engineering, the author is grateful for their critical review of the thesis.

The author appreciates the excellent work done by Mr. Homer Bates, Principal Laboratory Mechanic, in constructing the experimental model.

The author is indebted to the School of Civil Engineering and the Environmental Resources Center for assistance in publishing the dissertation as a technical report in the ERC series. Permission has been granted by the Graduate Division for special pagination and margins so that the dissertation could be published as such a report.

TABLE OF CONTENTS

TABLE OF CONTENTS (Continued)

LIST OF TABLES

LIST OF FIGURES

Figure | Page

TEXT

APPENDIX

LIST OF FIGURES (Continued)

NOMENCLATURE

A = full cross-sectional area of the sphere

dA = elementary projected area of the sphere

a = coefficient defined in Equation (A. 3)

a_i, $i=1,2$ = $\cos \varphi_i - \cos \varphi_0$, coefficients used for Equation (10)

b_i, $i=1,2$ = $\sin \varphi_i - \sin \varphi_0$, coefficients used for Equation (10)

C = couple

C_C = $C/(\zeta K r)$, couple coefficient

C_C^* = couple coefficient associated with C_I

C_D = $F_D/(\zeta K)$, drag coefficient

C_D^* = drag coefficient associated with C_I

C_D' = drag coefficient for free falling sand grains

C_F = $M_F/(\zeta K r)$, coefficient of the weight-restoring moment at the final stage

C_I = $M_I/(\zeta K r)$, coefficient of fluid-driving moment, M_I

C_{IM} = maximum value of C_I for a given force system

C_L = $F_L/(\zeta K)$, lift coefficient

C_L^* = lift coefficient associated with C_I

C_R = $M_R/(\zeta K r)$, coefficient of static weight-restoring moment, M_R

C_{Ri}, $i=0,1,2$ = coefficients defined in Equation (8)

c_i, $i=1,2$ = $C_{Ri} - C_{R0}$, coefficients used for Equation (10)

C_δ = impulsive-moment coefficient defined in Equation (22)

D = diameter of the sphere

e = 2.73 ...., Napierian base

F = resultant fluid-dynamic force

F_D = drag force passing through the centroid of the sphere

F_L = lift force passing through the centroid of the sphere

F_R = reactional force from the base

g = gravitational acceleration

h = protrusion height of the sphere or the distance from the top of the sphere to the plate

I = virtual moment of inertia of the sphere in the fluid

K = $\pi D^2 \rho u_T^2/8$, reference force parameter

k = Nikuradse sand-grain diameter

L = Laplace transform operator

M = magnitude of the positive net-driving moment

M_D = fluid-driving moment

M_F = static weight-restoring moment at the final stage

M_f = fluid-damping moment

M_I = static weight-restoring moment at the initial stage or the moment level which exceeds the fluctuating fluid-driving moment 95 per cent of the time

M_R = Wr sin φ, static weight-restoring moment

M_δ = impulsive moment

m = ratio of the negative net-driving moment to the positive net-driving moment

N_s = sediment number, defined in Equation (32)

n = total number of time increments of the sample

P_M = cumulative probability distribution of the fluid-driving moment, M_D

p = pin height above the base

R = radius of the sphere

r = effective rolling radius or the shortest distance between the centroid of the sphere and the rotating axis

s = parameter used in Laplace transform

T = total sampling time

t = time

t_0 = duration of positive net-driving moment

t_e = excursion time of the sphere

t_i, $i=1,2,\ldots n$ = incremental contact time

$\underline{t}$ = t/t_0, time in dimensionless form

U = unit step function defined in Equation (A. 2)

u = velocity of flow

u_b = bottom velocity of flow

u_T = flow velocity at the protrusion height, h

u_δ = representative flow velocity defined in Equation (31)

V = mean flow velocity

W = immersed weight of the sphere

w = half of the width between the sphere-pin contact points

y = distance above the boundary

y_0 = depth of flow

z = half of the clearance between the neighboring uniform spheres

α = angle of inclination of the bed

$\beta, \dot{\beta}, \ddot{\beta}$ = angular displacement, velocity, and acceleration of the sphere, respectively

γ = specific weight of the fluid

γ_s = specific weight of the sphere or sediment grains

δ = distance from the protrusion height, h, to the height of the representative velocity, u_δ

ζ = momentum correction coefficient defined in Equation (30)

η = factor defined in Equation (29)

$\Theta(s)$ = Laplace transform of $\underline{\theta}(t)$

$\theta, \dot{\theta}, \ddot{\theta}$ = small perturbed angular displacement, velocity, and acceleration of the sphere, respectively

θ_s = static equilibrium angle

$\underline{\theta}$ = dimensionless angular displacement defined in Equation (A. 5)

ν = kinematic viscosity of the fluid

ξ = constant

π = 3.1415 ....

ρ = density of the fluid

τ = boundary shear stress

φ, Φ = angle of repose

$\varphi_i, \Phi_i, i=0,1,2$ = angle of repose defined in Equation (8)

φ_M = angle of repose corresponds to C_{IM}

ω_0 = initial angular velocity of the sphere

SUMMARY

The mechanics of the process by which a sediment particle is removed from a stream bed was investigated. An idealized model, consisting of a one-inch diameter sphere protruding through a flat plate, a sphere-supporting base, and two equal height sphere-restraining pins aligned perpendicular to the flow direction, was used to simulate the condition of a cohesionless particle lying on a stream bed. By means of this model, the statistical variables of the angle of repose, the protrusion condition, and the approach velocity distribution became controllable at deterministic values.

In spite of the replacement of most of the statistical variables by the deterministic variables, initial motion of the particle is a fluctuating phenomenon which must be described in probabilistic terms because the fluid-dynamic force is fluctuating in nature. The transition from a stationary state to the removal of the spherical particle was found to be gradual rather than instantaneous. The transition is characterized by the random rocking motion of the sphere. The initial stage of the transition is defined as the condition at which the cumulative per cent time of contact between the sphere and the base is 95 per cent. The final stage is defined as the condition at which the sphere would be rolled over definitely. The condition of initial stage is established by equating the static weight-restoring moment to a moment level which exceeds the fluctuating fluid-driving moment 95 per cent of the time. The final stage is established by equating an additional impulsive moment to

the difference of the driving moment and the restoring moment as used in establishing the initial stage. The flow condition associated with the transition is expressed in terms of the mean velocity at the height of the protruding sphere. The effect of non-uniform velocity distribution is accounted for by the use of a momentum correction coefficient.

The fluid-dynamic moments and forces were determined experimentally in air flow with both uniform and non-uniform approach velocity profiles. Since the transitional stage is associated with the balance of moments, a method has been developed using the weight-restoring moment at the transitional stage as a gauge to measure the unknown fluid-driving moment. The corresponding fluid-driving force pattern was then determined through a set of three algebraic equations defining the equilibrium of moments due to the driving force and the restoring force. Experimental results indicated that the ratio of the coefficient of lift to drag decreased from approximately 1.6 to 0.4 as the ratio of the protrusion height to the sphere diameter increased from 25 per cent to 100 per cent. Also, the resultant fluid-driving force could be considered as passing through the centroid of the sphere for protrusion height equal to or less than 75 per cent of the sphere diameter.

CHAPTER I

INTRODUCTION

Sediment transport occurs by intermittent movement of individual bed particles in the fluid stream.* Of course, only the surface particles protruding into the fluid stream are subject to removal from the bed. Depending upon the turbulence in the stream and the settling velocity of the particle, some of the removed particles may have a high probability of a trajectory into the main body of the fluid stream before coming to rest again on the surface of the bed. Conversely some removed particles have a low probability of movement into the main stream and will roll, slide, or bounce along over the surface of the bed before coming to rest again. Based upon this distinction, sediment transport is classified as suspended load or bed load. Irrespective of the trajectory during movement, sediment transport is limited to the rate that sediment particles can be removed from the surface of the bed. The probability that an individual grain will be removed from the surface of the bed depends upon the geometry of the grain, upon protrusion above the mean bed level, upon position of bearing points with underlying particles (angle of repose), upon submerged weight, upon the hydrodynamic

*The exception to intermittent movement is the movement of particles so small or so nearly buoyant that these particles are non-settling. Sediment transported as non-settling particles is called wash load. Particles which are transported as wash load are absent from the bed of a movable bed stream. Thus sediment transport as used here refers to bed-material load.

force exerted on the surface of the particle by the fluid, and upon the probability of the surface grain being dislodged by another moving particle. Because each of the variables listed above is a statistical variable, formulation of models to represent sediment transport is and will remain a challenge.

Formulation of sensible models, either through mathematical or experimentally determined functions, requires an understanding of the physical process particularly in regard to the relative importance of the independent variables. In order to establish the relative importance and the effect of the independent variables, the independent statistical variables have to be controlled preferably at deterministic values. To simplify the problem of particle removal from a bed surface, many studies have been performed in which dislodgement of surface grains by other moving grains is precluded. Quite logically the removal of surface grains in the absence of other moving grains is called 'incipient motion.' While incipient motion is generally visualized in reference to the beginning of sediment transport, the probability of incipient motion of a bed particle could well be the central concept of sediment transport provided that particle dislodgement by other moving particles is a minor effect in the pickup of sediment grains from the bed surface.

Among the existing methods, there are two general approaches toward the formulation of incipient motion condition for noncohesive sediment: the critical-tractive-force approach and the critical-velocity approach.

The best known treatise on critical tractive force was published by Shields (28) in 1936. In his theoretical analysis, a functional relationship between the flow and the sediment was proposed as follows:

> The ratio of the effective force of water parallel to the bed to the resistance of a grain on the bed is a universal function of the ratio of the grain size to the thickness of the laminar boundary layer.

Shields then related these dimensionless parameters by experimental methods for the case with level bed and uniform particle size. White (32) made a similar analysis by considering the balance of the moments due to drag and immersed weight. Since then, many investigators have obtained results similar to Shields but with somewhat different numerical values for the dependent parameter. A general review on this matter was given by Vanoni (31).

Critical velocity is evaluated by recognizing that the fluid driving force is proportional to the square of the local flow velocity and the projected area of the particle. Mavis and Laushey (21) used the balance between the tractive force of the flow and the weight resisting force of the particle to establish a competent velocity formula under conditions of incipient motion. Allen (2) formulated theoretically and experimentally the stability criteria of blocks, broken stones and sands in stream flow, in terms of flow velocity. Novak (24) also investigated the stability of prisms on the bottom of a flume similar to the work of Allen. In his study of equilibrium of talus blocks downstream of stilling basins, Naib (22) established critical velocity formulae for both sliding and overturning in the light of lift and drag measurements. Neill (23) formulated his critical-velocity criterion from the standpoint of dimensional analysis. He also compared his formula with the previous design curves and formulae. Also, Goncharov (12), Ippen and Verma (14) and Carstens, Neilson and Altinbilek (5) developed critical velocity criteria by considering the balance of moments due to the drag and lift forces of the flow and the

immersed body force of the particle.

The purpose of the present study is to investigate the process of removal of an individual particle from the underlying bed and to formulate the conditions under which the particle undergoes a transition from a stationary state to an entrainment state. The transitional conditions of particle removal will be expressed in terms of the velocity in the vicinity of the protruding particle, rather than in terms of the bed shear stress. The use of a velocity parameter is considered to be more nearly universal inasmuch as velocity distribution is susceptible to either experimental measurement or analytical determination in non-uniform and/or unsteady flows whereas bed shear stress is extremely difficult to determine under these conditions. In fact, bed shear stress can not be measured directly even in uniform steady flow.

In order to determine the individual effects of the independent variables of particle protrusion, angle of repose, and approach velocity distribution a simplified model was chosen to approximate a protruding surface particle on the bed of a stream. In this study the movement of a single spherical particle was observed. The spherical particle was restrained from sliding in the direction of flow by two pins of equal height which were aligned perpendicular to the direction of flow. By adjusting the height of the pins, the angle of repose became a controllable deterministic independent variable. Because the base and supporting pins, upon which the sphere rested, could be moved with respect to the flat level plate over which flow occurred, protrusion was a controlled deterministic variable. The approach velocity distribution was controlled by means of a wire grid placed upstream from the

particle.

In spite of the replacement of most of the independent statistical variables by the independent deterministic variables, initial motion of the particle is a fluctuating phenomenon which must be described in probabilistic terms because the fluid dynamic surface force is fluctuating in nature.

CHAPTER II

PROBLEM FORMULATION

In order to understand the mechanics of particle removal in a flowing stream, a detailed examination of the force system acting upon the sediment particle is essential. The relationship between the flow characteristics and the sediment properties at the beginning of particle removal can then be determined from the knowledge of the force system involved. For a non-cohesive, granular particle immersed in a moving fluid, the forces which determine particle motion are the resultant fluid driving force, the particle restoring force, and the reaction forces from the contact with other surrounding particles.

The fluid-driving force is the resultant of shear stress and pressure over the surface of the particle. This resultant force is usually resolved into a drag force in the direction of the approach flow and a lift force normal to the flow direction. In general, both the force magnitude and line of application vary with time in turbulent flow. Even for laminar flow past a bed particle, the driving force may fluctuate. Kalinske (19) considered the eddies shed behind the particle as the cause of force fluctuation in a laminar flow field whereas Grass (13) related the shear stress fluctuation in laminar sublayers to the turbulence of the background flow close to the boundary. In addition to time dependency, the fluid driving force varies with the approach velocity profile, the particle protrusion conditions, and the shape and size of the particle.

The particle restoring force, for non-cohesive granular particles, is the immersed weight of the particle. The intergranular reaction forces act through a single axis of contact on neighboring particles as the particle rolls.* If the axis for the angular momentum equation coincides with the axis about which rolling occurs, the intergranular forces do not appear in the angular momentum equation.

A. Equation of Motion of the System

In order to study the response characteristics of a sediment particle subject to dynamic fluid driving loads, an idealized sphere-pin model as shown in Figure 1 is chosen. The model consists of a sphere, two equal-height pins, and a supporting base. The sphere is lying on a plane horizontal base and the movement of the sphere is restricted to rotation without slipping about the axis, O-O, of sphere-pin contact points.

When a particle undergoes angular acceleration through a fluid, a moment is required to accelerate the particle and an additional moment is required to accelerate some mass of the fluid set into motion by the particle. The moment of inertia associated with the mass of the fluid set into motion by the particle is called the added moment of inertia. The moment of inertia of the particle plus the added moment of inertia of the fluid is the virtual, or effective, moment of inertia of the particle in the fluid.

Since the sphere rotates about the axis of its contact with the pins without

---

*Although a sediment particle may be picked up from the bed by the lift force alone, as observed by Thompson (29), the general mode of the particle removal from a bed is the rolling motion of the particle about the points of contact with the supporting particles.

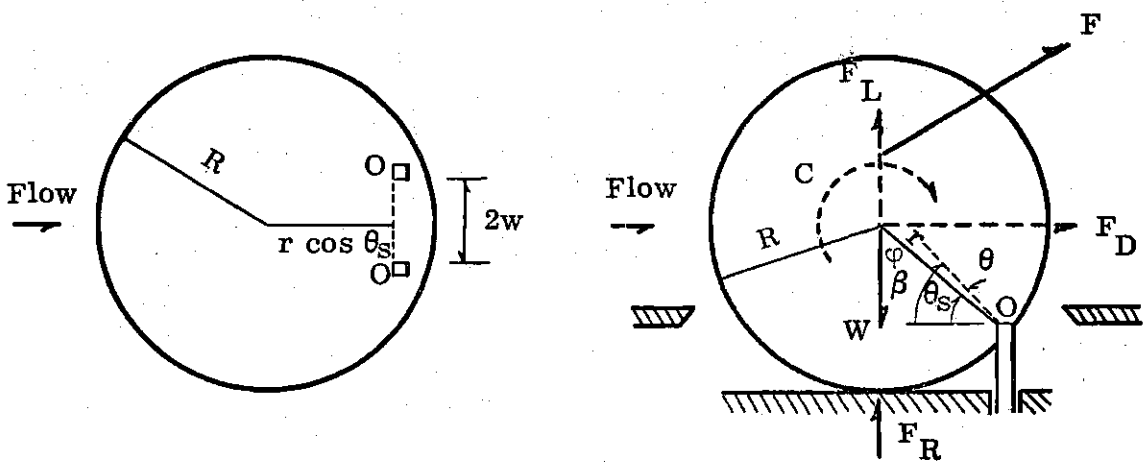

Top View Side Elevation

Figure 1. Force System on the Sphere-Pin Model.

slip, an equation of angular motion, as given below, will be sufficient to describe the general motion of the sphere.

$$I\ddot{\beta} = M_D - M_f - W r \cos\beta + F_R r \cos\beta \qquad (1)$$

in which, I is the virtual moment of inertia of the sphere in the fluid with respect to the axis of rotation, O-O; β is the angular displacement of the sphere measured positive clockwise from the horizon; $\ddot{\beta}$ is the corresponding angular acceleration; r is the shortest distance between the centroid of the sphere and the rotating axis O-O which by geometry is $(R^2 - w^2)^{\frac{1}{2}}$, where w is half of the width between the contact points; W is the immersed weight of the sphere; and F_R is the reactional force from the base. The left-hand side of Equation (1) is the product of the virtual moment of inertia of the sphere in the fluid and the angular acceleration of the sphere. The terms on the right-hand side of Equation (1) from left to

right represent the moment due to fluid-driving force, the fluid-damping or resisting force, the weight-restoring force of the sphere, and the ground-reactional force, respectively. In Equation (1), the angular displacement, β, can not be less than the static equilibrium angle, θ_s, due to the presence of the supporting base. The static equilibrium angle, θ_s, is the angle between the rolling arm, r, and the horizon when the sphere is at rest on the supporting base. By geometry, θ_s is equal to arcsin (R-p)/r, in which p is the height of the pins above the base and R is the radius of the sphere.

The moment associated with the reactional force can be eliminated from Equation (1) inasmuch as $F_R = 0$ whenever $\beta > \theta_s$.

$$I\ddot{\beta} = M_D - M_f - Wr \cos \beta \tag{2}$$

The weight-restoring moment, Wr cos β, decreases as the displacement β increases.

The nonlinear term cosβ associated with the weight-restoring moment in Equation (2) can be linearized for rocking motion with small displacement by considering the angular displacement $\beta(t)$ as the sum of a constant static equilibrium angle, θ_s, and a time-dependent angular displacement, $\theta(t)$,

$$\beta(t) = \theta_s + \theta(t) \tag{3}$$

For small angular displacement, $\sin \theta \simeq \theta$ and $\cos \theta \simeq 1$ resulting in

$$\cos \beta \simeq \cos \theta_s - \theta \sin \theta_s \tag{4}$$

Substituting Equations (3) and (4) into Equation (2),

$$I \ddot{\theta} + M_f - (Wr \sin \theta_s)\, \theta = M_D - Wr \cos \theta_s \tag{5}$$

Here, the weight-restoring moment has been decomposed into two terms: a constant term, $Wr \cos \theta_s$, associated with the static equilibrium angle, θ_s, and a linearized time-dependent term, $(Wr \sin \theta_s)\, \theta$, associated with the perturbed displacement, θ. Since $Wr \sin \theta_s$ is always positive, the negative sign before the perturbed restoring-moment term again indicates this restoring moment reduces as θ increases (17). The right-hand side of Equation (5) is the net driving moment applied to the sphere.

B. Determination of Fluid-Dynamic Moment and Forces

In general, the fluid-dynamic forces and moments acting on a solid body can be either indirectly determined by integrating the measured pressure distribution around the body surface or directly determined with the aid of a balance system (mechanical balances or strain-gage balances).

Particle removal can occur only when the net driving moment, right-hand side of Equation (5), is positive. Conversely, whenever the net driving moment is negative the particle will remain on the bed or will rotate back toward the bed. The limiting condition, when the net driving moment crosses from negative to positive is simply a condition of static equilibrium in which $F_R = 0$. Because the net

driving moment varies with time, the limiting condition must be interpreted statistically. For example, the beginning of particle removal is defined herein as the situation in which the net driving moment is positive 5 per cent of the time. For static equilibrium three independent equations are satisfied, that is, (1) the summation of the vertical forces equal zero, (2) the summation of the horizontal forces equal zero, and (3) the summation of the moments equal zero. Instead of experimentally measuring the lift and drag forces directly, a much simpler experimental method is to make three independent determinations of the limiting condition (moment) from which the equilibrium conditions can be used to calculate lift and drag. The three independent experimental measurements can be made by determining θ_s at the beginning of particle motion with spheres which differ only in weight in the same flow field.

In the past, O'Brien and Morison (25) applied a similar concept in determining the wave force exerted on a submerged spherical object. Young (33) also utilized the concept of force balance to determine lift and drag forces exerted on a spherical particle resting on the bottom of a sloping cylindrical tube. However, Young's proposition that the friction force vanishes at the condition of impending lifting motion is questionable and his measurement was restricted to laminar flow conditions only. In their study for establishing a length criterion for the hydraulic jump, Behera and Qureshy (4) determined the length of jump as the distance from the toe to the section where a cylinder placed on the floor of the flume would just topple. They felt the length criterion should be closely related to the scouring action and the transportation of sediment; and that the effects of all

the intricate forces could be measured with a fair degree of accuracy by placing a small cylinder in the flow after the jump.

In the present study, however, direct observation of the incipient motion phenomenon for an individual particle reveals that the particle undergoes a random rocking motion, without being physically rolled, for a range of differences between the fluid-driving moment and the particle-restoring moment. The duration of particle rocking above the bed floor increases as the difference between the driving moment and the restoring moment increases. Eventually, the particle will roll over after a critical angular impulse has been reached. There is no definite condition at which a stationary bed particle is placed in motion suddenly.

Although previous works in the field of sediment incipient motion are mainly based on the concept of static equilibrium, there are many investigators who did recognize the important role played by the fluctuating force on particle removal. In analyzing the critical condition for the motion of sand and gravels in rivers, Prandtl (26) states that whether a particle remains stationary or is swept away depends upon the largest force occurring in turbulent fluctuations, rather than the mean force. Thompson (29) has reported that the force exerted upon a stone on the stream bed is fluctuating in nature. He also asserted that the 'impulsive' force is responsible for the incipient motion of gravels in streams.

White (32) observed the maximum fluctuating velocity above the sediment grain to be about twice the mean and hence estimated the maximum drag is four times the mean for turbulent flow, whereas the maximum drag is twice the mean if the sediment is immersed in the laminar sublayer. Kalinske (19) has indicated

that the velocity fluctuation in turbulent flow near the bottom of rivers is distributed in accordance with the normal error law and the ratio of standard deviation to the mean is about one-fourth. He considered the shear stress at three standard deviations above the mean as the maximum shear in practice and thus concluded the maximum shear is about three times the mean value since shear varies as the square of the velocity. Einstein and El-Samni (10) observed that the pressure fluctuations at the top and the bottom of a hemisphere, lying on a stream bed consisting of identical hemispheres, are irregular and only a statistical description of these fluctuations appeared to be adequate. A careful statistical analysis showed that the probability distribution of the instantaneous pressure difference between the top and the bottom of the hemisphere, or lift forces at the stream bed, can be approximated by the normal error law. In a wind tunnel study of the nature of the forces on soil grains by wind, Chepil (8) found that the probability distribution of the fluctuating pressure of lift and drag followed a somewhat skewed normal-error law. The ratio of the mean pressure to the standard deviation was constant for various grain sizes and fluid velocieies. This ratio was found roughly equal to two. Chao and Sandborn (6) and Tieleman and Sandborn (30) have shown the randomness of the pressure fluctuations around a single sphere and around a sphere resting among identical roughness elements in turbulent flow.

In a theoretical and experimental study of the beginning of sediment motion, Gessler (11) utilized the armoring phenomena of non-cohesive sediment mixtures to determine the fluctuating pattern of the bottom shear stress exerted by the flow. He assumed that the fluctuations of the bed shear stress are distributed according

to the normal error law and that a grain is set into motion when the effective momentary shear stress acting on the grain exceeds a critical value which is a function of the Reynolds Number of the grain. Furthermore, he defined the critical shear stress for a particular grain as the average bottom shear stress of the stream flow when the probability of eroding of that grain size is equal to the probability of remaining still. Based on the above propositions, he concluded from the experimental measurements that the fluctuations of the bed shear stress are statistically distributed according to a Gaussian normal law. The ratio of the standard deviation to the mean was determined to be 0.57 as compared to a value of 0.5 used by Einstein (9) in his bed-load transport formula. By the use of a statistical treatment, Gessler was able to establish a systematically definable relation for the beginning of sediment motion. However, Gessler's definition of critical shear stress, for a particular grain size, as the average bed shear stress at which the probability of a grain being eroded is one-half is incorrect. This definition would be correct only if the response of the grain to the flow excitation is instantaneous and static in nature. Following Gessler's argument, when the mean bed shear stress is equal to the critical shear for a particular grain, the probability for the grain to be eroded is 50%. This in turn implies 50% of the fluctuating shear stresses exceed this critical shear level, according to his assumption that a grain is eroded when the effective shear stress exceeds the critical shear stress. However, for a dynamic system of sediment grain subject to fluctuating loads, the fact that the fluctuating shear exceeds the critical shear with 50% probability does not imply that the probability of the grain's being eroded is also 50%. In fact, a grain may be set into

motion with 50% probability of occurrence when the instantaneous shear stress exceeds a critical shear level other than the average shear.

In Cheng's work (7), a force dynamometer was used to measure the lift and drag forces exerted on a one-foot diameter sphere, embedded with identical particles, by the stream flow. Statistical analysis shows that the probability densities of the fluctuating lift and the drag forces are normally distributed. However, the standard deviations of both the lift and the drag are not constant as was proposed by Einstein (9) and Gessler (11). Instead, the standard deviations vary with flow conditions. In his study of incipient motion of a sphere, Cheng observed that the mean hydrodynamic forces do not necessarily have to exceed the weight of the sphere to cause motion. Rather, an instantaneous excess of force above the weight may be capable of removing the sphere. Apperley (3) has made transducer measurements of force components on a $\frac{1}{4}$-inch-diameter sphere with various protrusions above a flat bed of similar particles due to a turbulent water flow of 9 inch depth. The frequency distribution of the fluctuating drag and lift shows a skewed normal distribution. In the study of initial instability of fine bed-sand well immersed in a laminar sublayer, Grass (13) was able to determine the distribution of instantaneous bed shear stresses from knowledge of the instantaneous longitudinal velocity gradient inside the viscous sublayer adjacent to the boundary. The velocity profile was obtained through a high-speed camera tracking of the progress of a hydrogen bubble tracer in space and time. The instantaneous bed shear stresses also show a skewed normal distribution.

All these investigations either directly or indirectly support the idea that the

pressure field or the resulting force acting upon a three-dimensional roughness element on a stream bed is random in nature. The randomness of the particle rocking motion before roll-over can thus be reasoned as the particle response to the randomly fluctuating fluid-driving loads. The statistical regularity of the random response and excitation also suggests that the instability phenomenon associated with the beginning of particle removal can be better defined and understood through probabilistic considerations.

1. Probability Distribution of the Fluid-Driving Moment

Direct observation of the sphere at the transition of removal indicates the random motion of the sphere follows a statistically regular pattern. Measurements of pressure or forces acting on a bed element subject to stream flow also indicate this regularity in the fluctuation pattern (7, 8, 10). This significant behavior of statistical regularity has led to the assumption that both the fluctuating fluid-driving moment and the response of the sphere are stationary random processes. By 'stationary' we imply that the probability distribution of a random process is invariant to a shift of time origin of the sampling.

For the purpose of determining the fluctuating fluid-driving moment pattern, the sphere is assumed to be displaced above the static equilibrium position when the net driving moment applied to the sphere is greater than zero, or $M_D - Wr \cos \theta_s \geq 0$. In other words, the cumulative per cent of time the sphere, during its rocking motion, contacts the base is equal to the cumulative per cent of time that the given static weight-restoring moment exceeds the fluctuating fluid-driving moment. This assumption of equivalence between the response and the excitation of the sphere-pin

system can be expressed by:

$$P_M[M_D(t) \leq Wr \cos \theta_s] \simeq \sum_{i=1}^{n} t_i / T \qquad (6)$$

in which, P_M is the cumulative probability distribution of the fluid-driving moment, $M_D(t)$, $\sum t_i$ is the summation of the incremental contact time, t_i, during which $M_D \leq Wr \cos \theta_s$ or $\beta = \theta_s$ from the first to the last increment of the sample, and T is the total sampling time which must be large enough so that a statistically significant number of samples is made.

The principle used in determining the statistical information concerning the fluid-driving moment is illustrated by Figure 2. In Figure 2, the fluid-driving moment, $M_D(t)$, is shown as a random function of the time, t, and the static weight-restoring moment is shown as a time-independent constant crossing the fluctuating driving moment at a moment level of $Wr \cos \theta_s$. In reality, the duration at which the angular displacement, $\beta(t)$, exceeds θ_s is longer than the duration at which the fluctuating driving moment, $M_D(t)$, exceeds $Wr \cos \theta_s$ due to the time lag of the response.* In other words, the cumulative per cent time of contact is less than the cumulative probability of the driving moment, $M_D(t)$, being less than $Wr \cos \theta_s$. The incremental contact durations between the sphere and the base are shown in Figure 2 as solid lines at the angular displacement, θ_s. However, when the static weight-restoring moment crosses the fluctuating fluid-driving moment at high

*Deterministic analysis of the dynamic response of the sphere-pin system subject to idealized impulsive loads, based on the linearized equation of angular motion - Equation (5), are shown in Appendix A.

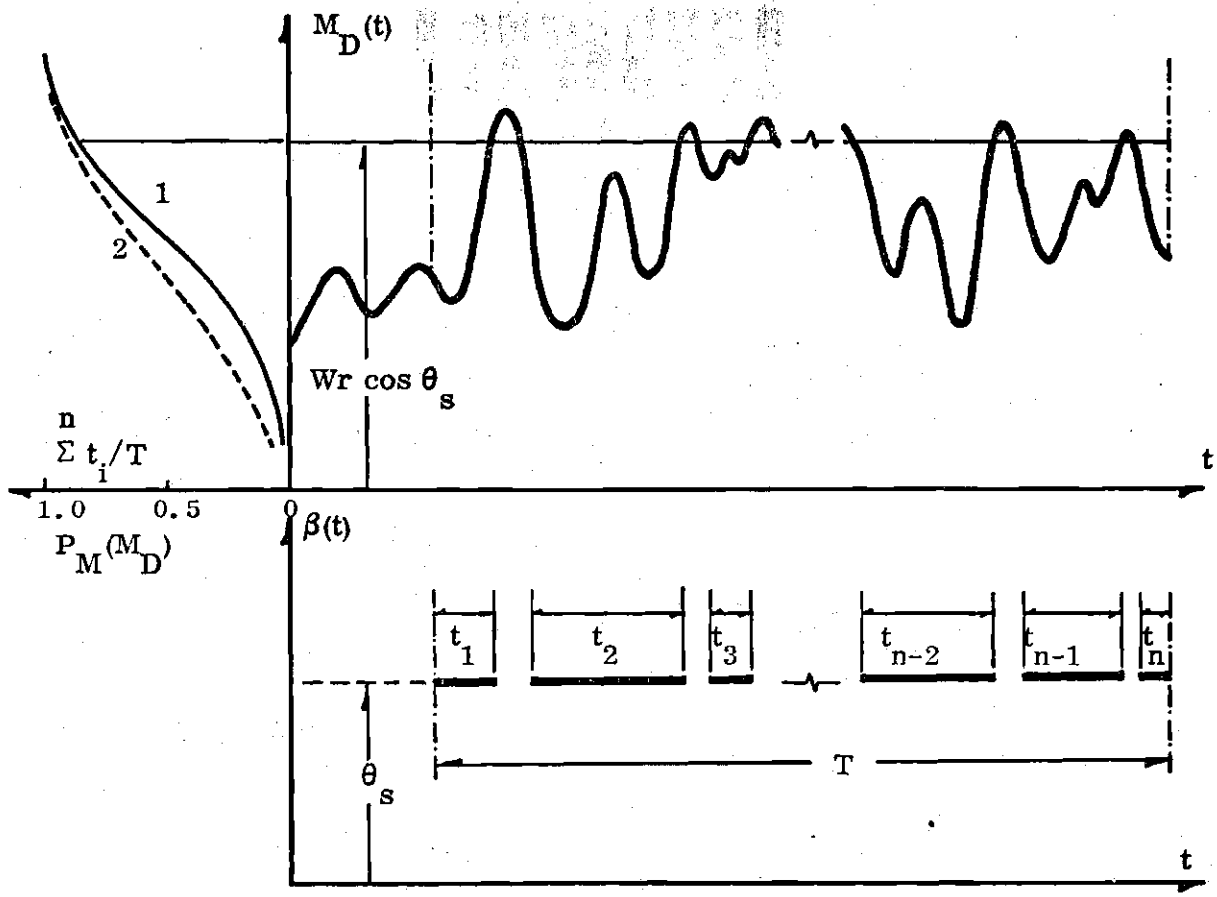

Curve 1 is the cumulative per cent time of contact between the sphere and the base at various levels of the weight-restoring moment, Wr cos θ_s.

Curve 2 is the cumulative probability distribution of the fluid-driving moment, M_D.

Figure 2. Method of Determining the Probability Distribution of the Fluctuating Fluid-Driving Moment.

moment level, as is shown in Figure 2, the proposition of Equation (6) is generally valid since the cumulative lag time between the response and the excitation is very short as compared to the cumulative time of contact.

Based on the proposition of Equation (6), the displacement of the sphere, $\beta(t)$, is equal to the static equilibrium angle, θ_s, or the sphere is in contact with the base when the static weight-restoring moment exceeds the fluctuating fluid-driving moment. The cumulative probability of the fluctuating fluid-driving moment which is below the moment level of a known restoring moment can then be readily determined experimentally by measuring the per cent of time that the sphere is in contact with the base.

The per cent time of contact is determined from the reading of an electric clock, which runs whenever the sphere is in contact with the metal-plated base, in reference to another clock reading which registers the total sampling time. The static weight-restoring moment, $Wr \cos \theta_s$, can be varied accurately by injecting liquids of different densities into the stainless steel hollow sphere. The hollow sphere is filled in full to avoid possible sloshing effect. In this way, the restoring moment is changed without altering the characteristics of the fluid driving moment. The cumulative probability distribution of the fluctuating driving moment can thus be obtained from the cumulative per cent time of contact, by systematically varying the level of the weight-restoring moment while maintaining the fluid-driving moment unaltered.

In Figure 2, the measured cumulative per cent time of contact versus the weight-restoring moment is shown as curve 1 and the cumulative probability

distribution of the fluid-driving moment is shown as curve 2. At high moment level, the cumulative per cent time of contact is representative of the cumulative probability of the fluid-driving moment. At lower moment levels, the cumulative per cent time of contact deviates from the cumulative probability of the driving moment.

2. Pattern of Fluid-Driving Force

If the sphere-pin system is subjected to an idealized steady fluid-driving moment, then the sphere would be barely lifted above the ground when the fluid driving moment barely overcomes the static weight-restoring moment. For a sphere-pin system subject to a fluctuating fluid-driving moment, both the response and the excitation are considered to be stationary random processes. At the beginning of the transition, the sphere performs a random rocking motion with very small displacements. Therefore, the condition at which the sphere has a high probability of being in contact with the base (say 95 per cent of the time) can be treated as if the system is under static equilibrium in which the fluid-driving moment exceeds the static restoring moment with a corresponding probability (about 5 per cent of the time). The determination of the fluid driving force pattern can then be achieved through a set of three static-equilibrium moment equations.

The static fluid-driving moment, M_D, can be resolved into a couple, C, and moments due to a drag force, F_D, and a lift force, F_L, passing through the centroid of the sphere. These decomposed forces F_D and F_L and couple C are shown in Figure 1. The equation of angular motion of the sphere-pin system under static equilibrium conditions can thus be expressed as

$$C + F_D r \cos\varphi + F_L r \sin\varphi = Wr \sin\varphi \qquad (7)$$

in which, φ is the angle of repose and is related to the static-equilibrium angle, θ_s, by $\varphi = \frac{\pi}{2} - \theta_s$ for the case of horizontal bed; $Wr \sin\varphi$ is the static restoring moment. All clockwise moments are considered positive.

The drag force, F_D, the lift force, F_L, and the couple, C, are the three unknowns whereas the angle of repose, φ, the moment arm, r, and the immersed weight of the sphere, W, are the knowns in the static-equilibrium Equation (7). Experimentally, we can set up three static equilibrium conditions, subject to the same unknown fluid-driving force pattern, each equilibrium condition having different values of the angle of repose, φ, and different values of the weight, W. The three unaltered unknowns can thus be determined by solving the set of three simultaneous equations each associated with one static-equilibrium condition.

Equation (7) is normalized by dividing by a reference force parameter

$$K = A\rho u_T^2/2$$

in which, $A = \pi D^2/4$ is a reference area,* D is the diameter of the sphere, u_T is the reference approach velocity taken at a height equal to the top of the sphere, and ρ is the density of the fluid.

---

*Since the resultant force or moment applied to the sphere as a whole is of major interest, the full cross-sectional area of the sphere is chosen as a reference area.

By defining the following dimensionless coefficients,

$$C_D = F_D/(\zeta K) = \text{Drag coefficient}$$

$$C_L = F_L/(\zeta K) = \text{Lift coefficient}$$

$$C_C = C/(\zeta K r) = \text{Couple coefficient}$$

$$C_R = W r \sin\varphi/(\zeta K r) = \text{Weight-restoring moment coefficient}$$

in which r is the rolling radius or the shortest distance between the centroid of the sphere and the axis of sphere-pin contact points, ζ is the momentum correction coefficient taking into account the effect of non-uniform velocity distribution (see IV. A. 3), the set of three equilibrium equations can be written in dimensionless form as follows:

$$C_C + C_D \cos\varphi_0 + C_L \sin\varphi_0 = C_{R0} \tag{8a}$$

$$C_C + C_D \cos\varphi_1 + C_L \sin\varphi_1 = C_{R1} \tag{8b}$$

$$C_C + C_D \cos\varphi_2 + C_L \sin\varphi_2 = C_{R2} \tag{8c}$$

in which the subscripts i = 0, 1, 2 denote the number of the test set.

Eliminating the couple coefficient C_C, the above equations are reduced to two equations

$$(\cos\varphi_1 - \cos\varphi_0)C_D + (\sin\varphi_1 - \sin\varphi_0)C_L = C_{R1} - C_{R0} \tag{9a}$$

$$(\cos\varphi_2 - \cos\varphi_0)C_D + (\sin\varphi_2 - \sin\varphi_0)C_L = C_{R2} - R_{R0} \tag{9b}$$

Since all values, except C_D and C_L, are known from experimental measurements at the equilibrium conditions, after substituting

$$a_i = \cos \varphi_i - \cos \varphi_0$$

$$b_i = \sin \varphi_i - \sin \varphi_0$$

$$c_i = C_{Ri} - C_{R0}$$

$$i = 1, 2$$

values for C_D and C_L are obtained as follows

$$C_D = (c_1 b_2 - c_2 b_1)/(a_1 b_2 - a_2 b_1) \tag{10a}$$

$$C_L = (a_1 c_2 - a_2 c_1)/(a_1 b_2 - a_2 b_1) \tag{10b}$$

The unknown couple coefficient, C_C, can then be obtained by substituting the values C_D and C_L, determined from above, into the moment equilibrium equation, Equation (8).

$$C_C = C_{Ri} - C_D \cos \varphi_i - C_L \sin \varphi_i, \; i = 0,1,2 \tag{11}$$

C. Limits of Transition

Because of the random nature of the motion of a sphere subject to a fluctuating fluid-driving moment, there is no critical condition at which motion begins suddenly. In fact, the transition from a stationary state to the removal of a bed particle is gradual rather than instantaneous. The limits of this transition will

hereafter be referred to as stages, that is the initial stage at which the sphere starts random rocking motion and the final stage at which the sphere rolls over.

1. Initial Stage

The initial stage is defined as the condition at which 95 per cent of the time the sphere is in contact with the base, that is, $F_R > 0$.* In other words, 5 per cent of the time the sphere is not in contact with the base, that is, $F_R = 0$.

The condition of initial instability for a particle lying on a plane bed with slope α can be formulated, according to the definition, by equating the static weight-restoring moment, M_R, to a moment M_I which exceeds the fluctuating fluid driving moment 95 per cent of the time.

Assuming the moment M_I is directly proportional to the fluid density, ρ, the rolling radius, r, the square of the reference approach velocity, u_T, the momentum coefficient, ζ, and the reference area $\pi D^2/4$, then the fluid driving moment at the initial stage can be expressed as:

$$M_I = C_I \zeta \pi D^2 r \rho u_T^2/8 \qquad (12)$$

in which, C_I is the fluid-driving moment coefficient at the initial stage, ζ is the momentum correction coefficient to account for the effect of non-uniform velocity

---

*The choice of 95 per cent probability is based upon the following reasons:
(i) the initial stage is associated with high cumulative per cent time of contact between the sphere and the base; and
(ii) reliable experimental data of cumulative per cent time of contact are obtainable up to the maximum value of about 95 per cent.

distribution. The moment coefficient, C_I, is a function of the angle of repose, φ, and the particle protrusion condition.

The static weight-restoring moment, M_R, of the sphere lying on a plane bed with slope α is

$$M_R = (\gamma_s - \gamma) \frac{\pi}{6} D^3 r \sin (\varphi - \alpha) \tag{13}$$

in which, γ_s is the specific weight of the sphere, γ is the specific weight of the fluid, φ is the angle of repose, and α is the angle of inclination of the bed measured from the horizon being positive for a downward slope and negative for an upward slope. Figure 3 shows the moment balance condition schematically.

Equating M_I and M_R from Equations (12) and (13),

$$\zeta \frac{u_T^2}{[(\gamma_s/\gamma) - 1]gD} = \frac{4}{3} \frac{1}{C_I} \sin (\varphi - \alpha) \tag{14}$$

in which g is the gravitational acceleration. Equation (14) defines the condition at the initial stage of the transition.

2. Final Stage

Unfortunately the final stage can not be logically defined by the contact time with the base but necessarily involves another definition based upon the experimental method. In the experiment the pin height was reduced in small increments until the sphere rolled over the pins. At least ten repetitions of a roll-over determination were made. In order to analyze these experimental data within a rational framework, the following analysis is presented.

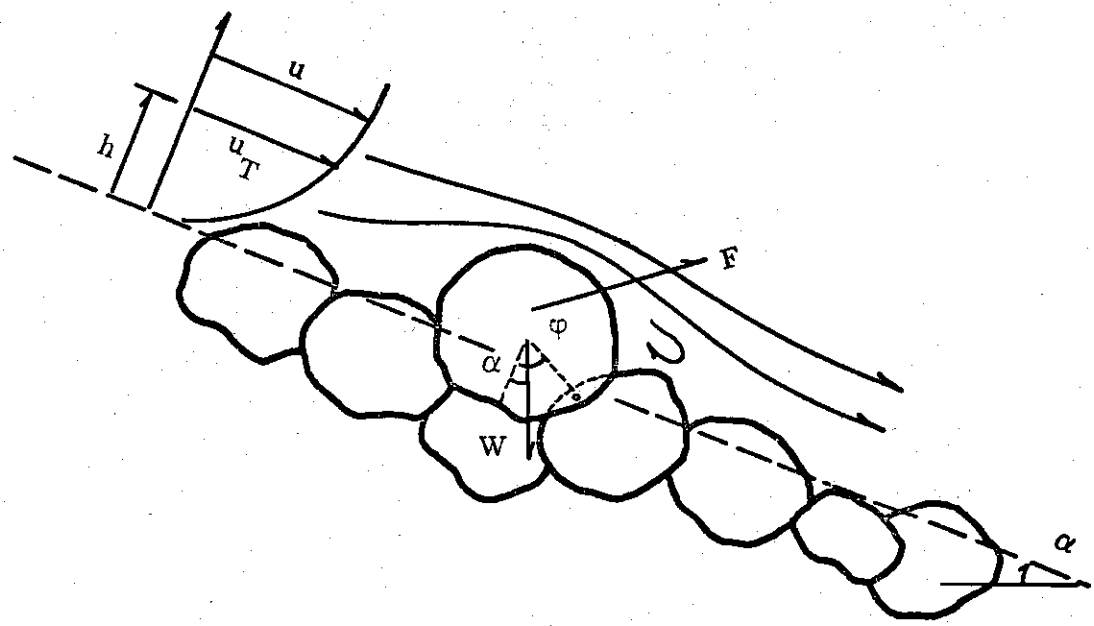

Natural Condition

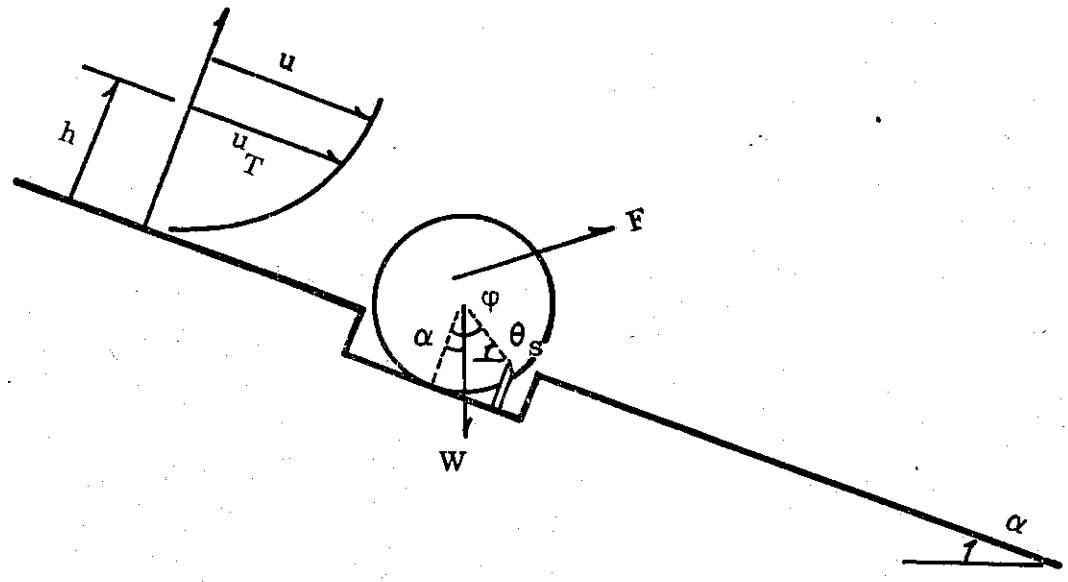

Idealized Model Condition

Figure 3. Stability Condition of Cohesionless Particle on Sloping Bed.

To study the motion of the sphere-pin system from the static equilibrium position to the roll-over position, the non-linear differential equation of motion, Equation (2), should be used since the displacement is no longer small. Considering

$$I\ddot{\beta} = -Wr\cos\beta \tag{15}$$

Multiplying both sides by the angular velocity $\dot{\beta}$,

$$I\dot{\beta}\ddot{\beta} = -(Wr\cos\beta)\dot{\beta} \tag{16}$$

Integrating Equation (16) and evaluating the constants of integration in terms of the initial displacement $\beta(0) = \theta_s$ and the initial velocity $\dot{\beta}(0) = \omega_0$, generated by an angular impulse,

$$I(\dot{\beta}^2 - \omega_0^2)/2 = -Wr(\sin\beta - \sin\theta_s) \tag{17}$$

The above equation represents the mathematical expression for the theorem of conservation of energy as applied to the sphere-pin system; the left side represents the change in kinetic energy, the right side represents the work done by the moment $(-Wr\cos\beta)$, or the change of potential energy.

The limiting condition for the sphere to reach its maximum height, or roll-over position, $\beta = \pi/2$, can be obtained by setting $\dot{\beta} = 0$ in Equation (17).

$$\omega_0^2 = 2Wr(1-\sin\theta_s)/I = 2Wr[1-\cos(\varphi-\alpha)]/I \tag{18}$$

in which $\varphi - \alpha = \frac{\pi}{2} - \theta_s$, φ is the angle of repose, and α is the angle of inclination

of the bed. Here ω_0 can be interpreted as the critical, or minimum, initial angular velocity required to achieve this critical roll-over condition.

Consider that this critical initial velocity ω_0 of the system is established as a result of the application of a critical angular impulse or a net impulsive moment M_δ over a very short period of time t_0 (in comparison with the time of traverse from $\beta = \theta_s$ to $\beta = \frac{\pi}{2}$).* Then, the following relation between ω_0 and M_δ can be obtained by the angular impulse-momentum principle:

$$I(\omega_0 - 0) = \int_0^{t_0} M_\delta \, dt \tag{19}$$

in which the sphere is assumed to be at rest on the bed before the application of the angular impulse. Assuming M_δ is constant over duration t_0, then

$$\omega_0 = (M_\delta / I) \quad t_0 \tag{20}$$

Substituting the above relation into equation (18),

$$M_\delta^2 = \frac{4IWr}{t_0^2} \sin^2 \frac{\varphi - \alpha}{2} \tag{21}$$

---

*If t_0 were of the same order as the time of traverse from $\beta = \theta_s$ to $\beta = \pi/2$, there would be no need of an additional angular impulse (or the resulting velocity ω_0) to roll the sphere over. With sufficient duration, the fluid driving moment which is barely equal to the static restoring moment will be able to roll the sphere over since the restoring moment decreases as the sphere rolls up (See II. A.).

Since $I = \xi(W/g)r^2$* where ξ is a constant,

$$M_\delta = C_\delta(\gamma_s - \gamma)\frac{\pi}{6}D^3 r \sin\frac{\varphi-\alpha}{2} \tag{22}$$

in which $C_\delta = 2\sqrt{\xi}/(\sqrt{g/r}\ t_0)$ is an impulsive-moment coefficient. Equation (22) indicates that the impulsive moment is directly proportional to the immersed weight of the sphere, the effective radius of rolling, and the sine function of $(\varphi - \alpha)/2$.

The final stage of transition can be expressed as

$$M_I - M_R \geq M_\delta$$

or

$$M_I - M_R \geq C_\delta(\gamma_s - \gamma)\frac{\pi}{6}D^3 r \sin\frac{\varphi-\alpha}{2} \tag{23}$$

In Appendix A, a positive square-wave net-driving moment which persists for a time, t_0, followed by a constant negative net-driving moment is utilized in Equation (5) to obtain a solution for the excursion time of the sphere. As shown in Table A.1, the sphere will roll over if the value of at_0 exceeds the limiting value delineated by the heavy-line curve. By definition of the coefficient a, the parameter, at_0, is inversely proportional to C_δ. The point is that the analysis presented in Appendix A reinforces the validity of C_δ as a significant parameter. Values of C_δ can be determined from experiments by means of Equation (23).

---

*While the effect of the added moment of inertia of the fluid is implicitly included in ξ and C_δ, the experiments were conducted in flowing air in which the effect of the added moment of inertia was negligible.

Substituting Equations (12) and (13), for the expressions of M_I and M_R, into Equation (23),

$$\zeta \frac{u_T^2}{[(\gamma_s/\gamma) - 1]\, gD} = \frac{4}{3} \frac{1}{C_I} \left[\sin (\varphi - \alpha) + C_\delta \sin \frac{\varphi - \alpha}{2} \right] \qquad (24)$$

Equation (24) defines the condition at the final stage of the transition.

CHAPTER III

EXPERIMENTS

The process of removal of an individual particle from a stream bed depends mainly upon the characteristics of the fluid-dynamic forces exerted on the protruding particle and upon the properties of the bed particles. Because of the fluctuating nature of the fluid-dynamic forces and because of the random pattern of the particle's rocking motion at the transition stage of particle removal, experiments were required in order to evaluate the fluid-dynamic forces. In these experiments, the weight-restoring moment of the particle was used as a gauge to determine the magnitude of the fluid-driving moment. The probability distribution of the fluctuating fluid-driving moment was evaluated by the per cent time of contact of the sphere with the underlying bed.

A. Apparatus

The experimental set-up for studying the process of particle removal and for determining the effects of the angle of repose, the particle protrusion, and the velocity distributions on particle removal, is shown in Figures 4 and 5. The sphere-pin model consists of a sphere, two equal-height pins aligned perpendicularly to the flow direction, and a supporting base for the sphere. The height of the pins in reference to the base can be adjusted to simulate the variation in the angle of repose. The level of the sphere-supporting base relative to a horizontal flat

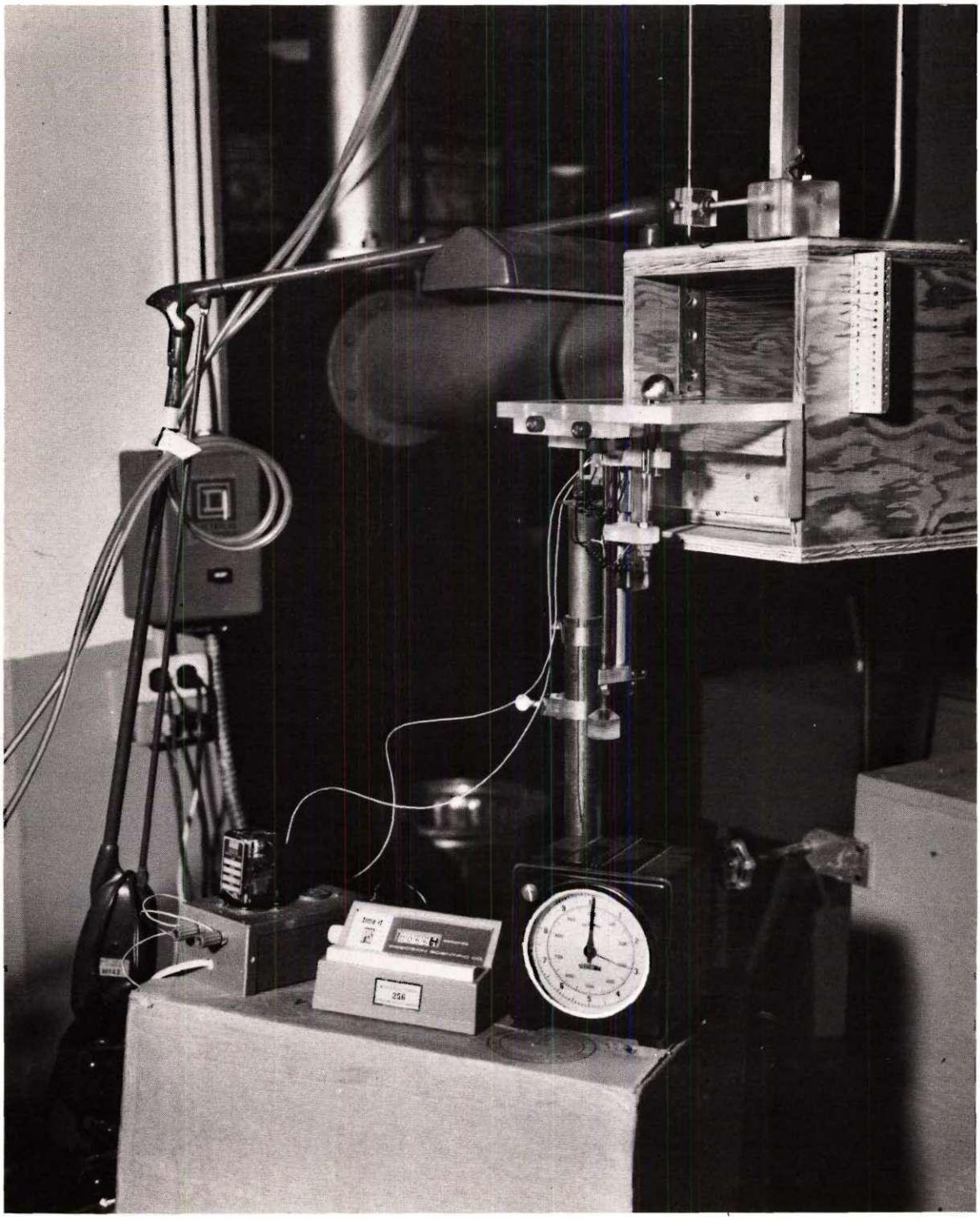

Figure 4. Photograph of Experimental Apparatus.

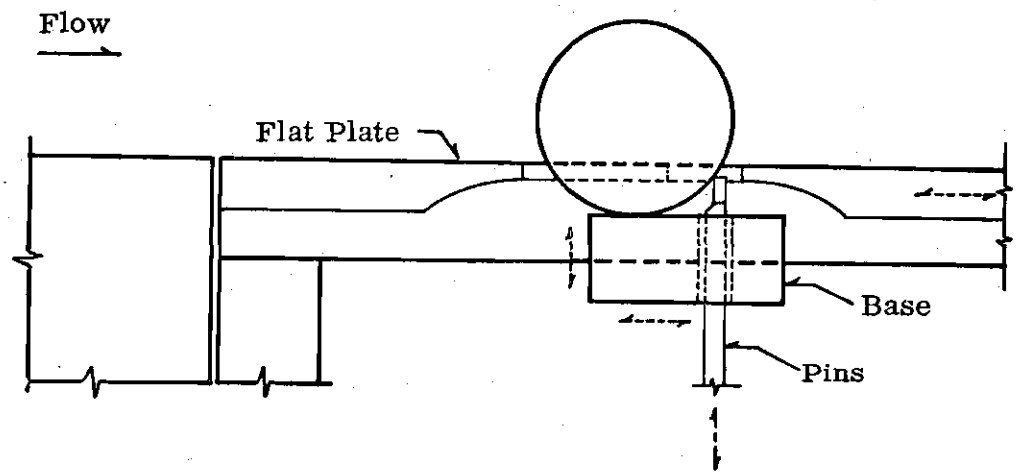

Section A-A

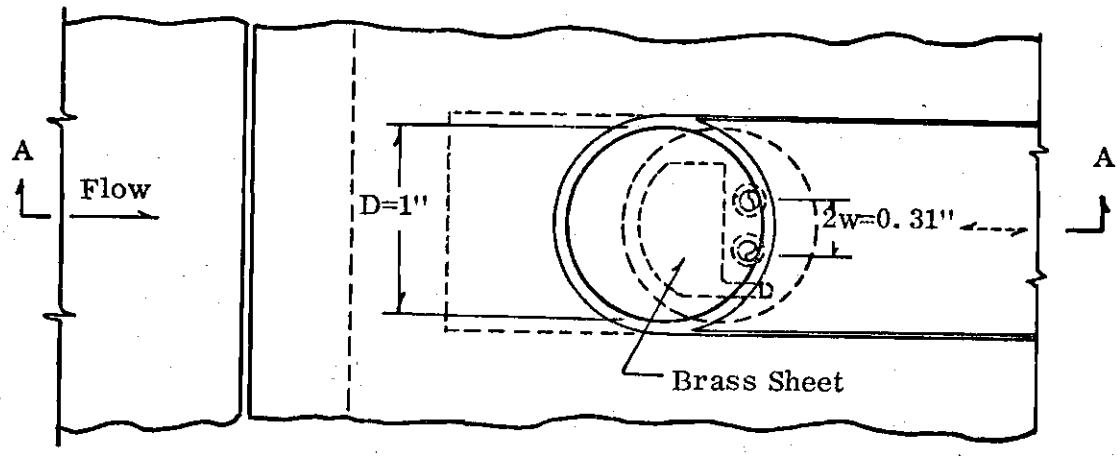

Plan

Figure 5. Sphere-Pin Model Arrangement.

plate over which the flow occurs can be controlled to simulate the variation of the particle protrusion above the bed. The horizontal flat plate is placed at the open end of a contraction section which is $7\frac{3}{8}$ inches in width by 4 inches in height. The air flow is directed to the contraction section from a 20-inch-wheel centrifugal air blower through a series of 90-degree guide vanes. The velocity of the air flow could be controlled by a variable speed selector aligned between the air blower and a 5-horsepower induction motor. The velocity distribution of the approach flow could be empirically generated by adjusting the spacing of a wire grid, placed at the end of the contraction section, upstream from the leading plate. The mean velocity profile at the front section of the leading plate could be determined by means of a movable Pitot-tube.

A one-inch diameter stainless-steel hollow ball was chosen as the test sphere. A very thin brass sheet was glued to the top of the sphere-supporting base. The cumulative time of contact between the sphere and the base could be registered by connecting electric circuits from the ends of the two steel pins and from the end of the brass sheet of the base to the input of an electronic relay, and connecting the output of the relay to an electric digital counter clock. The sphere which rocked against the pins served as a switch to actuate the relay. The relay actuated the counter clock. The circuit was closed when the sphere was in contact with the brass sheet of the base, and opened when it was not. The electronic relay served to reduce the maximum input circuit current to 5 milliamperes and thus avoided the possible error due to the arcing effect. The input sensitivity of the relay was 0-50 megohms and the relay response time was 10 milliseconds. The cumulative per cent time of

contact between the sphere and the base was obtained by using another electric timer clock which registered the total sampling time of the test. Variation of the weight of the test sphere was made possible by injecting liquids of different specific weights to fill up the hollow ball through a small machine-drilled hole of 0.018-inch diameter. Liquids with varying specific gravities from 2.96 to 0.78 were obtained from solutions of various concentrations of acetylene tetrabromide ($CH\ Br_2 \cdot CH\ Br_2$) in alcohol. Other heavy liquids, such as bromoform ($CH\ Br_3$), with a specific gravity of 2.86, and carbon-tetrachloride ($C\ Cl_4$) with a specific gravity of 1.58, were also mixed with alcohol to produce other solutions.

In performing experiments on the final, or roll-over, stage of particle removal, a series of one-inch diameter spheres made of different materials were used in addition to the hollow balls. A list of the materials of these balls and their corresponding weights is given in Table 1.

Table 1. Material and Weight of Different Test Spheres (1-inch diameter)

Material	Weight (grams)	Material	Weight (grams)
Stainless steel	66.57	Lexan	10.27
Aluminum	23.53	Acrylic	9.855
Glass	21.30	Nylon	9.85
Teflon	18.45	Stainless Steel (hollow)	7.08
Delron	12.065	Wood	6.52
Acetate	10.55	Wood chip	1.84

B. Procedure

Before starting each experiment, the desired particle protrusion was set by adjusting the level of the sphere-supporting base relative to the flat plate over which flow occurred. The desired approach velocity distribution was achieved by trial arrangement of the size and spacing of the horizontally fastened wire grids. The velocity profile was measured by a Pitot-tube traverse across the upstream section of the flat plate in the absence of the sphere. The angle of repose was calculated from the height, p, of the two vertical pins measured above the top of the brass sheet glued to the base, the radius, R, of the sphere, and the width, 2w, between the two pins.

An experiment was started with the heaviest possible weight of the sphere. With the sphere resting against the pins, the height of the pins was then adjusted to a value at which the cumulative per cent time of contact between the sphere and the base was greater than 95 per cent. With the pin height fixed, the cumulative per cent time of contact was obtained from the reading of the counter clock and that of the timer clock. The electric timer clock recorded the total sampling period whereas the electric digital counter clock registered the cumulative time of contact between the sphere and the base during the sampling period. The data of per cent time of contact for a fixed weight-restoring moment condition was generally taken from a set of nine or more samples. While the sphere was set in the testing position, three sets of samples (each with a 100-second sampling period) were obtained consecutively. Then, the sphere was removed from the base and reset in position

for another three sets of 100-second samples. This removal and reset process was repeated two or more times. This procedure of data sampling was mainly for convenience and reliability. However, the method was a good test for the stationarity of the random rocking motion since consistent results were obtained from the consecutive sampling. The distribution of the cumulative per cent time of contact under various weight-restoring moments was obtained by repeating the sampling process for different weight-restoring moment conditions. The weight-restoring moments were varied by incrementally changing the weight of the liquid mixture in the hollow sphere. Experiments for determining the distribution of the cumulative per cent time of contact were terminated at a restoring moment level at which either the cumulative per cent time of contact was very low, 5 per cent or less, or the sphere would roll frequently within the 100-second sampling period, whichever occurred first.

At each angle of repose, the same procedure for determining the distribution of cumulative per cent time of contact under various restoring-moment levels was repeated.

Experiments for determining the condition of the final or roll-over stage of particle removal were performed differently. With the test sphere in position, the pin height was lowered gradually in very small increments until the sphere would roll. Tests on roll-over conditions were also performed with one-inch diameter balls listed in Table 1 other than the stainless steel ball injected with liquid mixtures. Experiments to determine the roll-over condition for each fixed weight of the sphere were repeated ten or more times.

C. Results

All experimental results are presented in Appendix B. The experiments were conducted under both uniform and non-uniform approach velocity conditions. The velocity profiles for Run I, II, and III are shown in Figure B.1. Uniform velocities of 92.5 feet per second and 58.5 feet per second were generated for Run I and II, respectively. A non-uniform velocity profile was generated for Run III. The experiments covered a range of the particle Reynolds number, $u_T D/\nu$, from 3×10^4 to 5×10^4 where ν is the air viscosity. By defining the protrusion condition as the ratio of the height of sphere above the flat plate, h, to the diameter of sphere, D, a range of h/D from 25 per cent to 100 per cent was covered in the experiments.

Experimentally determined values of $W \sin \varphi$ or $C_R \zeta K$ as a function of the cumulative per cent time of contact are presented in Figures B.2 through B.11. Normal probability paper is used to facilitate the plotting. Values of $W \sin \varphi$ at the value of 95 per cent cumulative time of contact on these graphs are the values of M_I/r or $C_I \zeta K$. Values of $W \sin \varphi$ at the roll-over condition are designated as the values of M_F/r or $C_F \zeta K$. Values of $W \sin \varphi$ at the initial stage or M_I/r and values of C_I are listed in Table B.1. Values of $W \sin \varphi$ at the final stage or M_F/r and values of C_F are listed in Table B.2. Values of C_I and C_F as a function of φ are also shown in Figures 6 and 7.

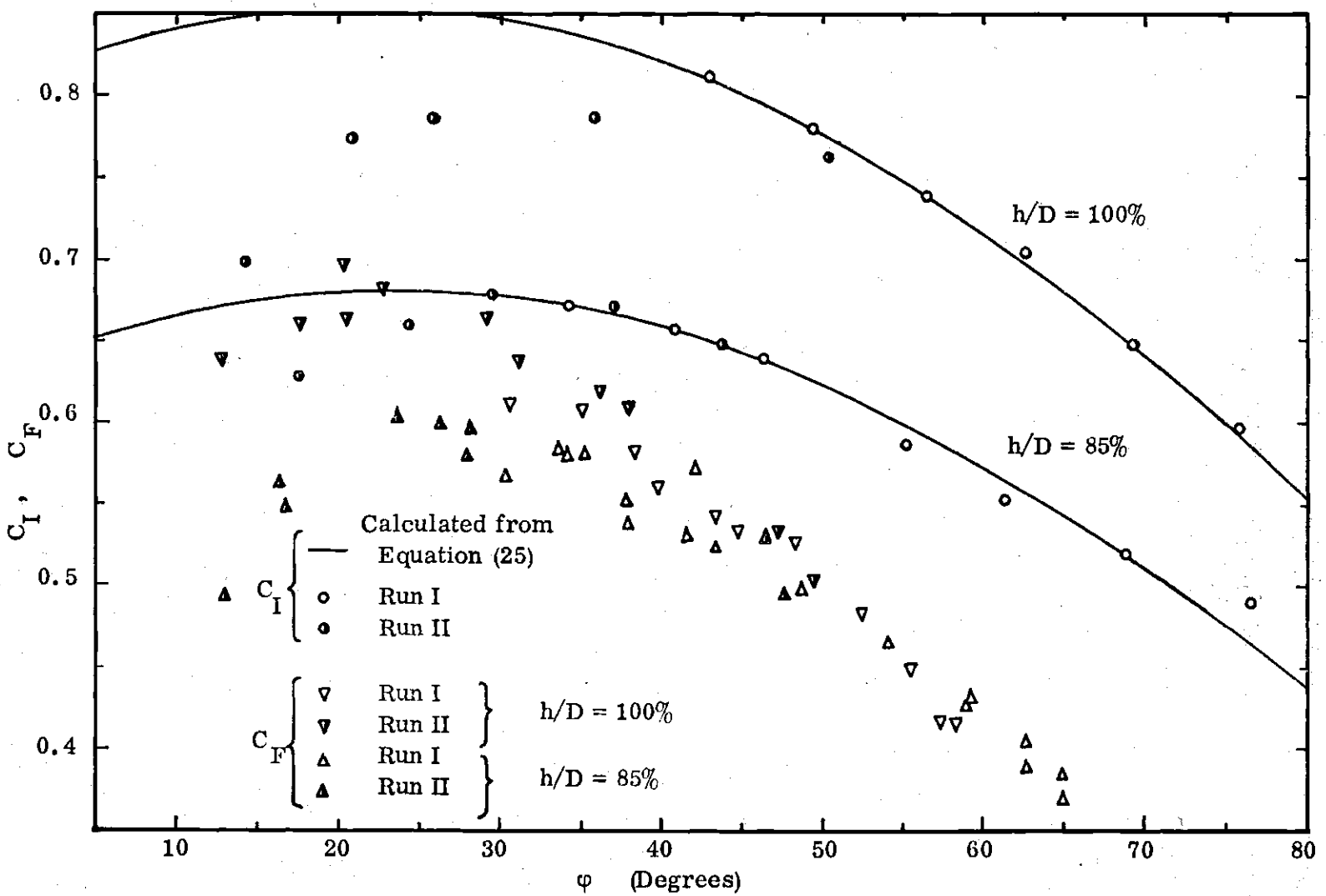

Figure 6. Moment Coefficients C_I and C_F for Protrusion Conditions of 100% and 85%.

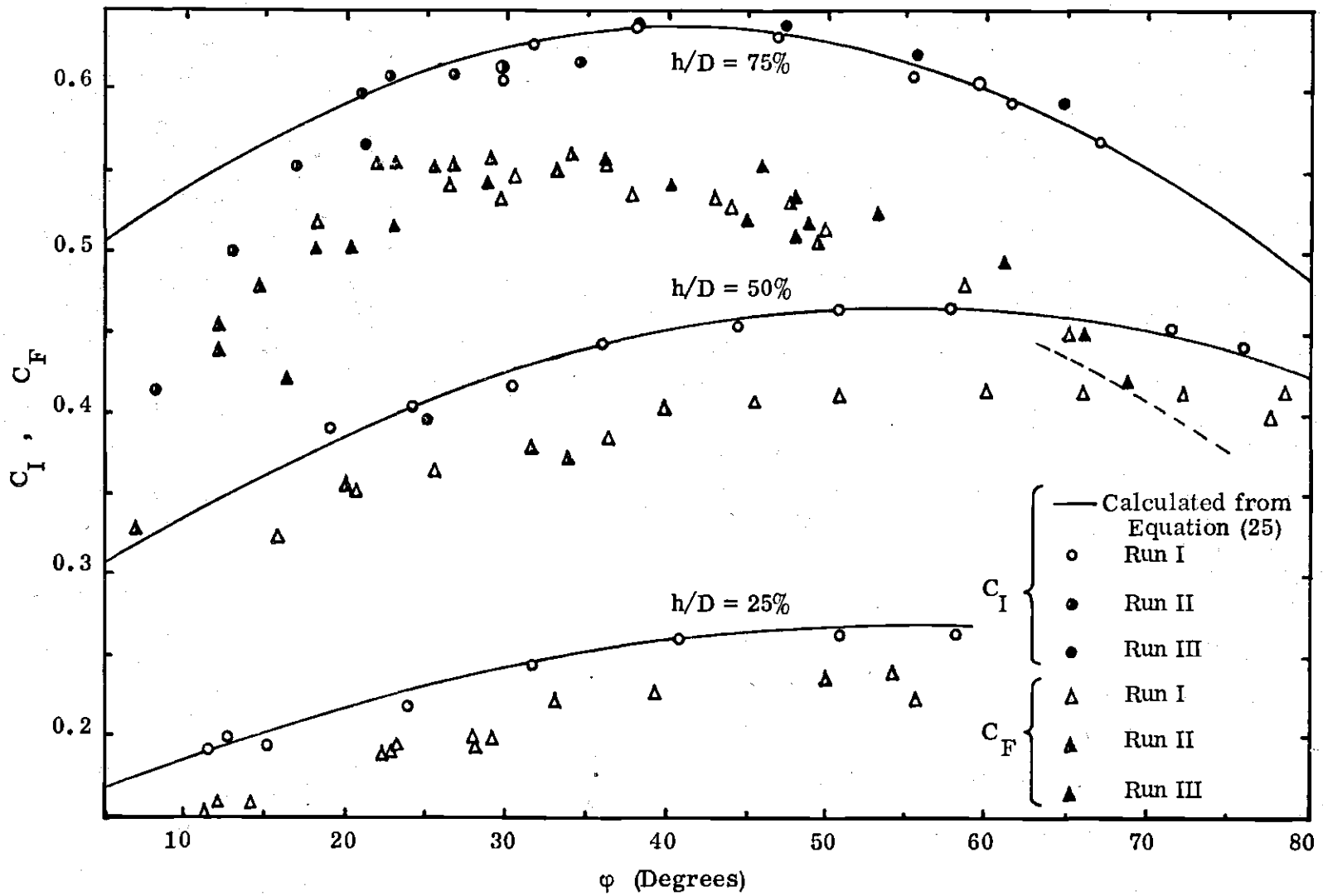

Figure 7. Moment Coefficients C_I and C_F for Protrusion Conditions of 75%, 50% and 25%.

CHAPTER IV

ANALYSIS OF RESULTS AND DISCUSSION

In all experimental runs, the measured points of the cumulative per cent time of contact at various levels of W sin φ follow approximately a straight line on the normal probability plottings shown in Figures B.2 through B.11. In the experimentally determined probability functions shown in Figures B.2 through B.11, M_D/r can be substituted for W sin φ when the cumulative per cent time of contact is large. On the other hand, M_D/r will be less than W sin φ whenever the cumulative per cent time of contact is small because in this range the time for the sphere to fall back to the base is appreciable. As a consequence, the experimentally determined probability functions can be used in the further analysis of the initial stage of transition but not for the analysis of the final stage.

A. Initial-Stage Analysis

The experimentally determined values of W sin φ at the initial stage are nearly equivalent to the fluid-driving moment (actually M_I/r) which is equalled or exceeded 5 per cent of the time. The characteristics of an equivalent steady-state force system which would produce M_I can be calculated by means of Equations (9), (10), and (11). A convenient representation of this equivalent force system is by means of the coefficients of drag, lift, and couple or C_D^*, C_L^*, and C_C^*, respectively. Typical computations for determining the equivalent force system at various

protrusion conditions using Equation (8) are shown in Tables B.3 through B.7. In the following sections, the effects of the angle of repose, the protrusion condition and the velocity profile upon the pattern of the coefficients of moments and forces will be examined.

1. Effect of Angle of Repose

Although the fluid-driving force pattern is independent of the angle of repose, the driving moment associated with a fixed force pattern is indeed a function of the angle of repose. The values of C_D^*, C_L^*, and C_C^* determined for the initial stage can then be substituted into Equation (8) to give a functional relationship between C_I and φ as follows.

$$C_I = C_C^* + C_L^* \sin\varphi + C_D^* \cos\varphi \qquad (25)$$

Computed values of C_I are also listed in Tables B.3 through B.7. These computed values of C_I as a function of φ are shown as solid-line curves in Figures 6 and 7.

The function, Equation (25), shown in Figures 6 and 7 is symmetrical about the maximum, C_{IM}. For a given force pattern, C_{IM} occurs when the moment arm with respect to the rolling axis is maximum or when the angle of repose is equal to the angle of the resultant force measured from the horizon. The angle of repose associated with C_{IM} is designated as φ_M. An alternative expression for Equation (25) in terms of C_{IM} and φ_M is

$$C_I = C_{IM} \cos(\varphi - \varphi_M) + C_C^* \qquad (26)$$

A summary of the values of C_D^*, C_L^*, C_C^*, C_{IM}, φ_M, and C_L^*/C_D^* as computed in

Tables B.3 through B.7 are listed in Table 2.

Table 2. Coefficients of Moment and Force, and φ_M at Various Protrusion Conditions

h/D (%)	C_{IM}	φ_M (degree)	C_D^*	C_L^*	C_C^*	C_L^*/C_D^*
100	.854	21.4	.592	.232	.219	.392
85	.680	23.6	.502	.219	.133	.437
75	.638	41.1	.523	.457	-0.056	.873
50	.466	54.9	.258	.367	.018	1.421
25	.270	57.2	.143	.222	.007	1.553

If the resultant fluid-driving force passes through the centroid of the sphere, the couple coefficient, C_C^*, would be zero. As shown in Table 2, C_C^* is small in relation to C_{IM}, for h/D equal to or less than 75 per cent.

2. Effect of Protrusion

To determine the effect of protrusion empirically, all values of C_{IM}, C_D^*, C_L^*, C_C^*, C_L^*/C_D^*, and φ_M as listed in Table 2 are plotted in Figure 8 as a function of h/D. The relationship between the moment coefficient, C_{IM}, the angle, φ_M, and the protrusion condition, h/D, can be expressed in the simplified forms as

$$C_{IM} \simeq 0.09 + 0.75\ h/D \qquad (27)$$

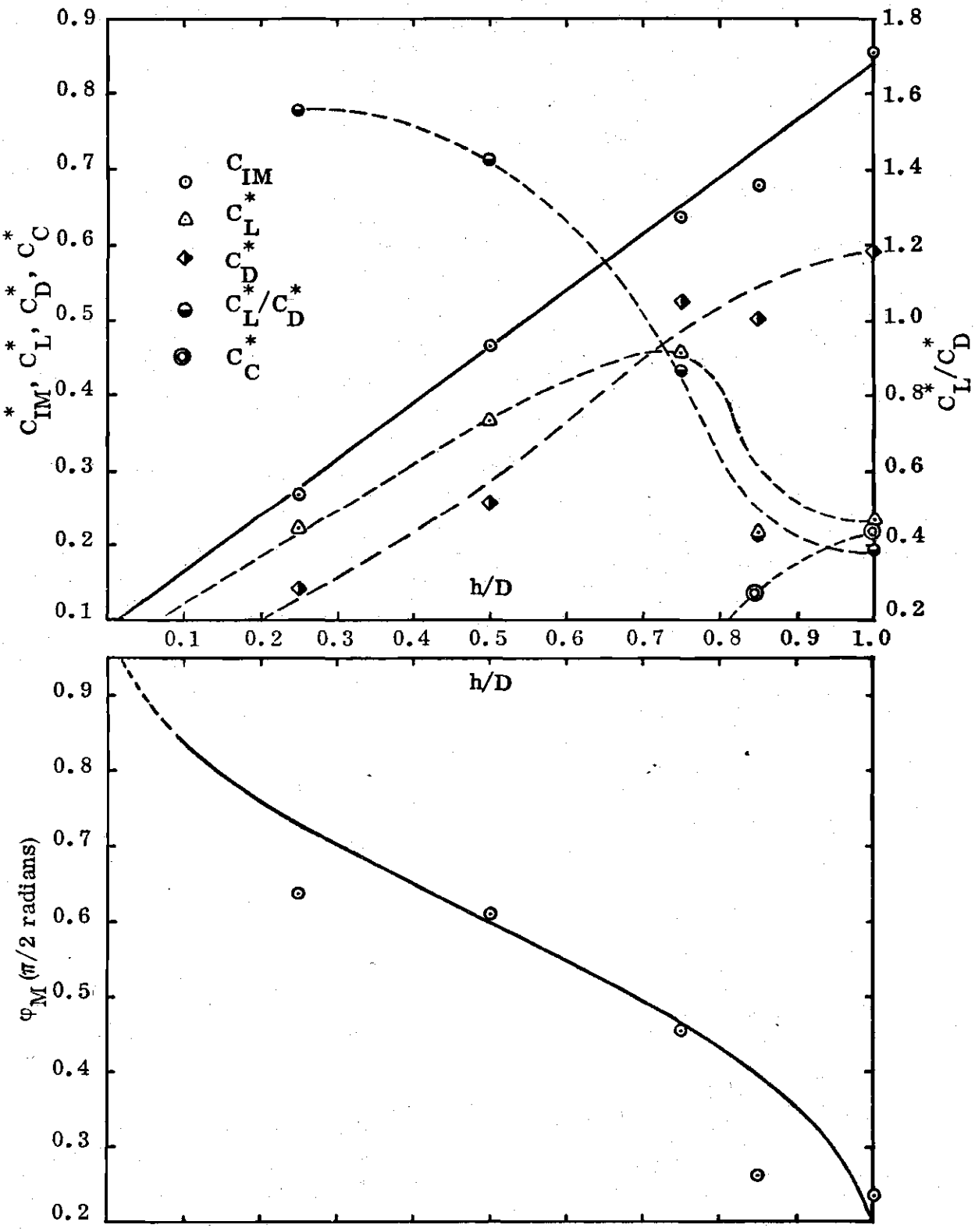

Figure 8. Effect of Protrusion on Moment and Forces.

and

$$\varphi_M \simeq 0.3\pi - 0.4 \arcsin(2h/D - 1) \qquad (28)$$

in which φ_M is expressed in radians. The variation of the force coefficients C_D^* and C_L^* as a function of h/D do not follow a simple trend. As h/D increases, the drag coefficient increases proportionately whereas the lift coefficient increases to a maximum value at approximately 75 per cent protrusion. The general pattern of the fluid-driving forces at various protrusion conditions are illustrated in Figure 9.

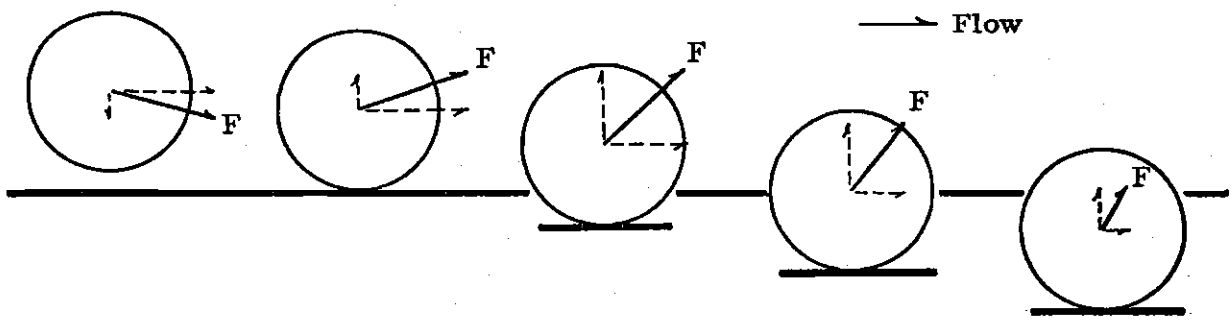

Figure 9. Force Pattern at Various Protrusion Conditions.

The reduction of lift coefficient, C_L^*, at protrusion conditions beyond 75 per cent is mainly due to the flow passage through the gap between the sphere and the plate which reduces the pressure at the bottom region of the sphere. In fact, at protrusions beyond 100 per cent, negative lift force was predicted theoretically by Jeffreys (18) and observed experimentally by Apperley (3).

Tieleman and Sandborn (30) have made a study of the effect of a single roughness element in a turbulent boundary layer of a smooth flat plate. The roughness

element, a 3/16-inch diameter sphere, was subject to air flow with non-uniform velocity distribution. The Reynolds number of the sphere, UD/ν, was approximately 3×10^3 if the free stream velocity, U, of 30 feet per second was used. In their study, pressure distribution around the surface of the sphere was measured. The average drag and lift forces on the sphere, computed by integrating the pressure distribution, were found to be 4.07×10^{-5} lbs and 0.86×10^{-5} lbs, respectively. Using the velocity profile measured by Tieleman and Sandborn at a distance 32 inches from the leading edge, an average drag coefficient of 0.39 and an average lift coefficient of 0.08 are obtained from Tieleman and Sandborn's study.

Early in 1939, Klemin, Schaefer, and Beerer (20) performed model study of a perisphere (a hollow spherical building) in a wind tunnel. The model sphere was 2 feet in diameter and was placed 0.08 feet above the ground board. The aerodynamic forces were measured by the conventional method of mechanical balances. At an air velocity, U, of 15 miles per hour, the corresponding Reynolds number, UD/ν, was approximately 3×10^5. For the case with the sphere supported by a collar on the ground board, the drag and lift coefficients were 0.57 and 0.42, respectively. For the case with the sphere supported by columns on the ground board, the drag coefficient was 0.49 and the lift coefficient was 0.25.

In the present study, coefficients C_D^* and C_L^* of 0.59 and 0.23, respectively, were obtained for the sphere with full protrusion. The Reynolds number, $u_T D/\nu$, is approximately 5×10^4. The results obtained by Tieleman and Sandborn (30) and by Klemin, Schaefer, and Beerer (20) are generally in agreement with those obtained in the present study.

In a study of air flow behind a hemisphere with 2.5 cm radius, Jacob (16) determined the drag force by integrating pressure distribution around the surface from which value of C_D of 0.22 was calculated. This value of the drag coefficient for the hemisphere again compares favorably to the value determined in the present study, that is, for a sphere with 50 per cent protrusion, $C_D^* = 0.26$.

3. Effect of Velocity Distribution

Assuming the magnitude of the fluid-dynamic force exerted upon an obstructing sphere is proportional to the rate of transfer of the approach fluid momentum, the force is then proportional to

$$\eta \int^{A} \rho u^2 d A \tag{29}$$

in which, u is the non-uniformly distributed approach velocity, and dA is the elementary projected area of the sphere normal to the flow direction, and η is the factor to account for other effects due to the non-uniformity of the velocity profile.

For convenience, the fluid-dynamic force can also be expressed as being proportional to the reference force parameter K, or $\frac{\rho}{2} u_T^2 A$. The expression, Equation (29), can be replaced by the product of the parameter K and the momentum correction coefficient, ζ, defined as

$$\zeta = \frac{\eta \int^{A} \rho u^2 dA}{K} = \frac{\eta \int^{A} u^2 d A}{\frac{1}{2} u_T^2 A} \tag{30}$$

Therefore, the coefficient of fluid-dynamic force defined as the ratio of the force to the product of ζ and K is expected to be independent of the profile of velocity

distribution.

In experimental Run No. III-1, a non-uniform approach velocity profile was generated. The protrusion condition of the sphere was 75 per cent. By choosing a value of 0.787 for ζ, the moment coefficient C_I as determined from test data of Run III-1 resulting in almost identical values of C_I as determined from the test data associated with uniform velocity profiles under the same protrusion condition of 75 per cent (Run I-9 and Run II-1). The computed values of C_I as a function of φ for both the uniform and non-uniform velocity profiles, are shown in Figure 7.

The value of ζ/η, obtained through numerical integration of Equation (28) for the case of Run III-1, is approximately 1.04. This implies a value of η equal to 0.76 for the protrusion condition of 75 per cent. Since only one experiment under non-uniform velocity condition was conducted in the present study, values of η for other protrusion conditions can not be established.

Alternatively, by choosing a representative velocity, u_δ, measured at a distance δ below the top of the protruding sphere such that,

$$\frac{1}{2}\rho u_\delta^2 A = \eta \int^A \rho u^2 d A \tag{31}$$

then the coefficient of fluid-dynamic force defined as the ratio of the force to the parameter, $\frac{\rho}{2}u_\delta^2 A$, will be independent of the effect of velocity distribution. The values of u_δ and δ/D for the data of Run III-1 are 70.6 feet per second and 0.32, respectively.

Previously, Carstens, Neilson, and Altinbilek (5) also proposed a representative height being 0.6 diameter above the bed, or approximately a distance, δ,

of 0.4 diameter below the top of a protruding particle. This finding was based on experimental study of the incipient motion condition of sand particles submerged within the laminar boundary layer of oscillatory flow over a flat bed.

4. Initial Stage

In the theoretical analysis of the process of particle removal, the condition for the initial stage of the transition is given by Equation (14). The fluid-driving moment coefficient, C_I, can be determined by means of Equation (25) together with the experimentally determined coefficients C_D^*, C_L^*, and C_C^* listed in Table 2. Alternatively, Equations (26), (27) and (28) can be used to evaluate C_I.

The conditions for the initial stage, at various protrusion conditions, are shown in Figure 10 as the solid-line curves. The abscissa of Figure 10 is the angle, $\varphi - \alpha$. The ordinate is expressed in terms of a sediment number, N_s, defined as

$$N_s = \sqrt{\zeta}\, u_T \Big/ \sqrt{[(\gamma_s/\gamma) - 1]\, gD} \qquad (32)$$

As shown in Figure 10, N_s increases as $(\varphi - \alpha)$ increases. Conversely, N_s decreases as h/D increases.

B. Final Stage Analysis

In order to determine the condition for the final stage of the transition, information concerning the characteristics of the impulsive-moment coefficient, C_δ, is required in addition to the values of coefficient of moment or forces determined in the initial-stage analysis.

Based on Equation (23) which defines the condition of moment balance at the

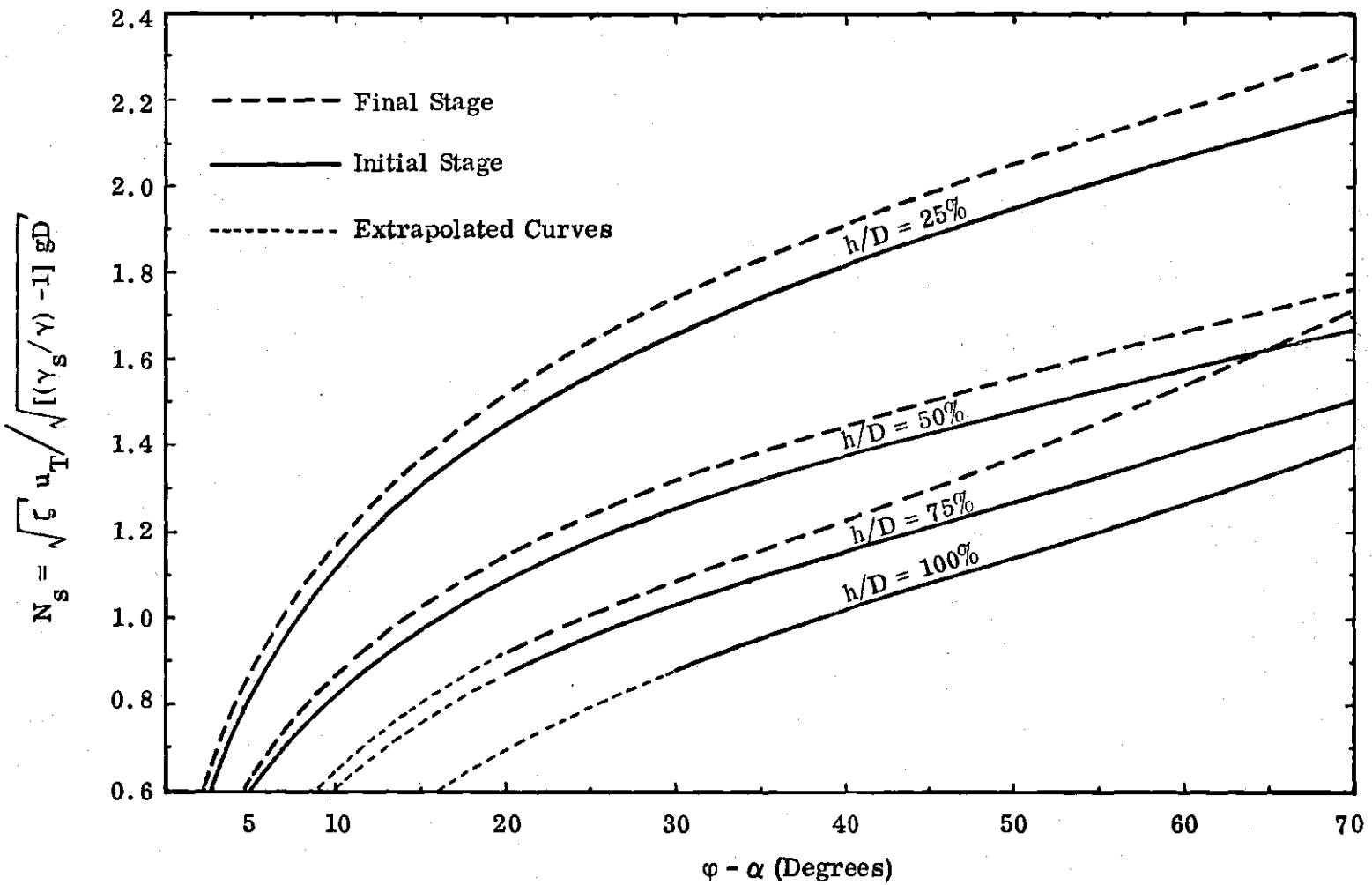

Figure 10. Transition of Particle Removal.

final stage, the impulsive-moment coefficient, C_δ, can be obtained as follows

$$C_\delta = (C_I - C_F)\, \zeta\, K/W \sin \frac{\varphi}{2}$$

The computed values of C_δ are tabulated in Table B.2.

1. Impulsive-Moment Coefficient

Computed values of the impulsive-moment coefficient, C_δ, are shown in Figure 11 for a range of φ from 20 degrees to 70 degrees. At 50 per cent protrusion, the computed values of C_δ vary from 0.2 to 0.3. At 25 per cent protrusion, C_δ varies from 0.2 to 0.4. By comparing the order of magnitude of the impulsive moment term, C_δ Wr $(\sin \frac{\varphi}{2})$, with the weight restoring moment term, Wr sin φ, in Equation (23), the scatter of C_δ has an insignificant effect in determining the condition of particle roll over. Since the final stage is defined as the condition at which the particle rolls over, the lower limiting value of $C_\delta = 0.2$ will be used for protrusion conditions equal to or less than 50 per cent. The lower-limiting value of C_δ can be considered as the minimum impulsive-moment coefficient required to establish the final stage. For particle protrusion beyond 50 per cent, there is a trend of increasing C_δ as the angle of repose is increased. The increase in C_δ is larger at higher protrusions. This effect of high protrusion upon the variation of C_δ can be explained by the following argument. In the analysis of impulsive moment for particle removal (see II. C. 2), the sphere is considered to be in contact with the base before being subjected to the angular impulse. However, this assumption is generally valid for low protrusion conditions but fails for high protrusion conditions. At high protrusions, the flow

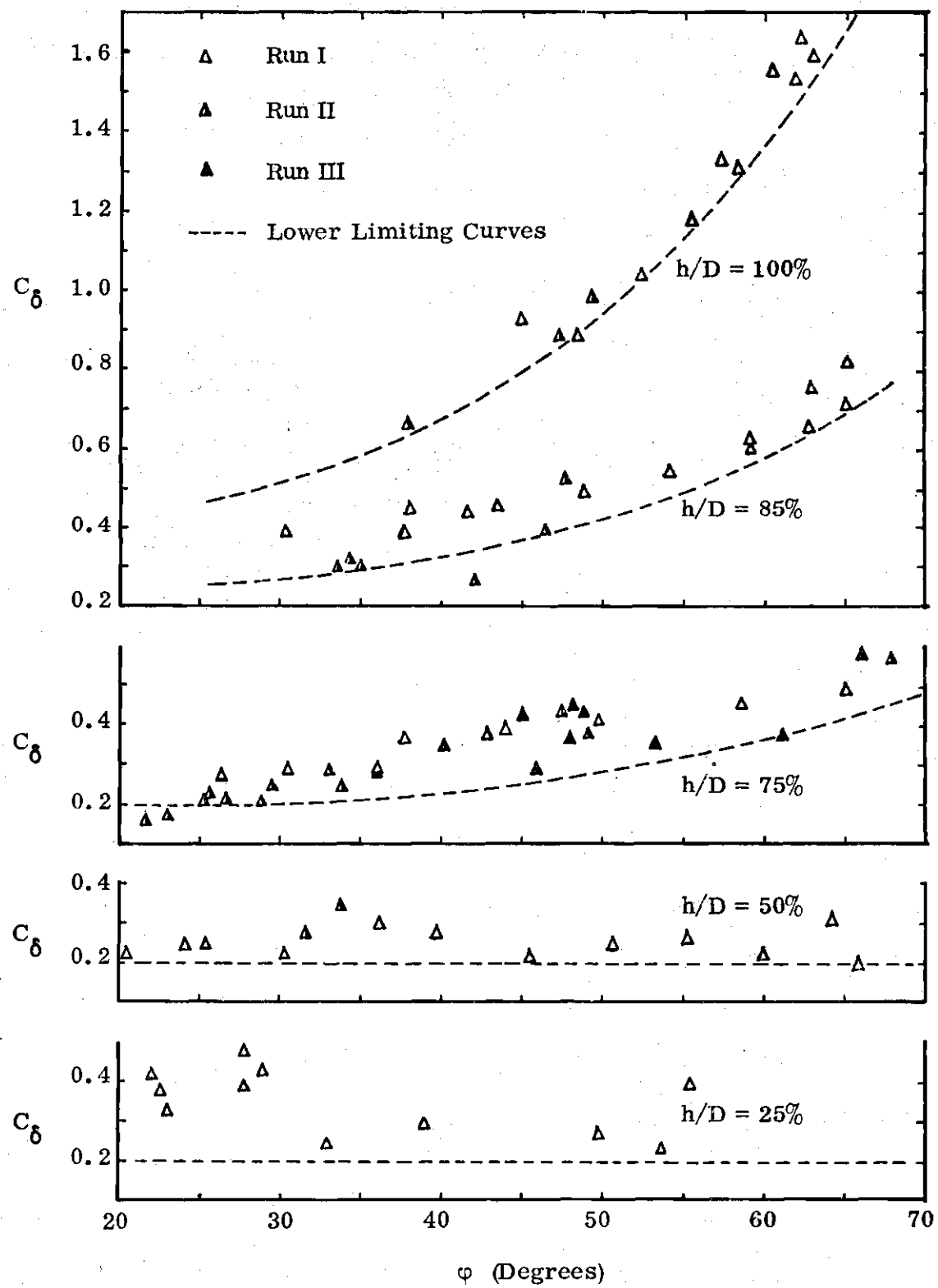

Figure 11. Impulsive Moment Coefficient.

field around the sphere changes as the sphere rolls above the base. The resulting fluid-driving moment is reduced as a result of lift-force reduction when the flow passage through the gap between the sphere and the base is increased. This reduction in fluid-driving moment thus requires less weight-restoring moment to maintain equilibrium. The reduction of weight restoring moment is then achieved naturally by establishing a smaller value of φ or a new equilibrium level at a distance above the base. The sphere will then be in equilibrium about this higher level until there is a strong angular impulse causing roll over. The computed values of C_δ at high protrusions has thus implicitly taken into account the effect of flow-pattern alteration before the occurrence of the final stage.

2. Final Stage

The condition for the final stage are defined by Equation (24) in which the fluid-driving moment coefficient, C_I, has been determined in the initial-stage analysis. The value of C_δ can be obtained from the lower-limiting values shown in Figure 11.

The conditions for the final stage, at various protrusion conditions, are also shown in Figure 10 as dashed-line curves.

It is interesting to note that the transitional range of N_s values between the initial and the final stage is rather narrow as compared to the values of N_s. This indicates the difference in N_s value due to the discrepancy in defining the stage of particle removal is not appreciable as compared to the other factors, such as φ and h/D.

C. Comparison

The validity of the present finding in determining the transitional conditions of particle removal will be examined by comparing the critical velocities for particle removal obtained by the author's method and by others' methods.

A steady, two-dimensional, uniform, open channel flow is considered. All other pertinent data are given below:

Water depth	$y_0 = 2$ ft
Channel slope	$\alpha \simeq 0$
Specific gravity of the particle	$\gamma_s/\gamma = 2.65$
Density of water	$\rho = 1.94$ slug/ft^3
Particle diameter	$D = 3$ mm

In order to determine the velocity distribution, the Karman-Prandtl equation (27) for turbulent flow over hydraulically rough boundaries is used.

$$\frac{u}{\sqrt{\tau/\rho}} = 2.5 \log_e \frac{y}{k/30} \tag{33}$$

in which, u is the velocity at a distance y above the boundary, τ is the boundary-shear stress, and k is the Nikuradse sand-grain diameter. The sand grain diameter, k, is taken equal to D by assuming uniform sizes of the bed materials. The mean velocity, V, across the depth, y_0, can be obtained through integration of Equation (33) from y = D/30, where u is zero, to $y = y_0$.

$$\frac{V}{\sqrt{\tau/\rho}} = 2.5 \left[\log_e 30 \frac{y_0}{D} - 1 + \frac{D}{30y_0} \right] \tag{34}$$

In the subsequent sections, the mean velocity, V, of the stream at which the bed material begins to move as determined by various methods will be presented for comparison.

1. Shields' Parameter (28,31)

The commonly used value of Shields' critical shear stress parameter, $\frac{\tau}{(\gamma_s - \gamma) D}$, for coarse sand is 0.06. The corresponding value of $\sqrt{\tau/\rho}$ is 0.177 ft/sec. The mean velocity, V, as obtained from Equation (34) is equal to 3.40 ft/sec.

2. Mavis and Laushey's Formula (21,31)

The empirical formula for determining the critical bottom velocity, u_b, as given by Mavis and Lauchey is

$$u_b = \frac{1}{2} \left(\frac{\gamma_s}{\gamma} - 1 \right)^{1/2} D^{4/9} \tag{35}$$

in which D is the particle diameter in millimeters and u_b is in feet per second. The bottom velocity is thus equal to 1.05 ft/sec. By assuming u_b occurs at y = D, then the corresponding mean velocity as obtained from Equations (33) and (34) is 2.38 ft/sec.

3. Neill's Criterion (23)

The mean-velocity criterion proposed by Neill is

$$\frac{\rho V^2}{(\gamma_s - \gamma) D} = 2.0 \left(\frac{D}{y_0}\right)^{-1/3} \tag{36}$$

From Equation (36), the critical mean velocity, V, is equal to 1.78 ft/sec.

4. Carstens, Neilson, and Altinbilek's Parameter (5)

The incipient motion criterion proposed by Carstens, et. al. is

$$\frac{u_\delta^2}{[(\gamma_s/\gamma) - 1] gD} = \frac{\tan \varphi \cos \alpha + \sin \alpha}{1 + \tan \varphi} \frac{8.2}{C_D'} \tag{37}$$

in which u_δ is the velocity at a position 0.6D above the bed and C_D' is the drag coefficient for free falling sand grains. At high Reynolds number, the value of C_D' for sand grains is approximately equal to 1.12 (1). For well rounded sand grains with a diameter of 3 mm, the angle of repose, φ, is generally taken as equal to 30 degrees. The velocity, u_δ, for the case of flat bed, or $\alpha = 0$, is evaluated to be 1.18 ft/sec. The corresponding mean velocity, V, as determined from Equations (33) and (34) with u = 1.18 ft/sec at y = 0.6D, is 3.16 ft/sec.

5. Author's Method

Considering an idealized arrangement of the protruding sphere lying on top of a layer of uniform spheres, as shown in Figure 12 below, the angle of repose of the protruding sphere is by geometry,

$$\varphi = \arctan \left[(1 + z/R)/2 \sqrt{3-(1 + z/R)^2}\right] \tag{38}$$

in which z is half of the clearance between the neighboring spheres.

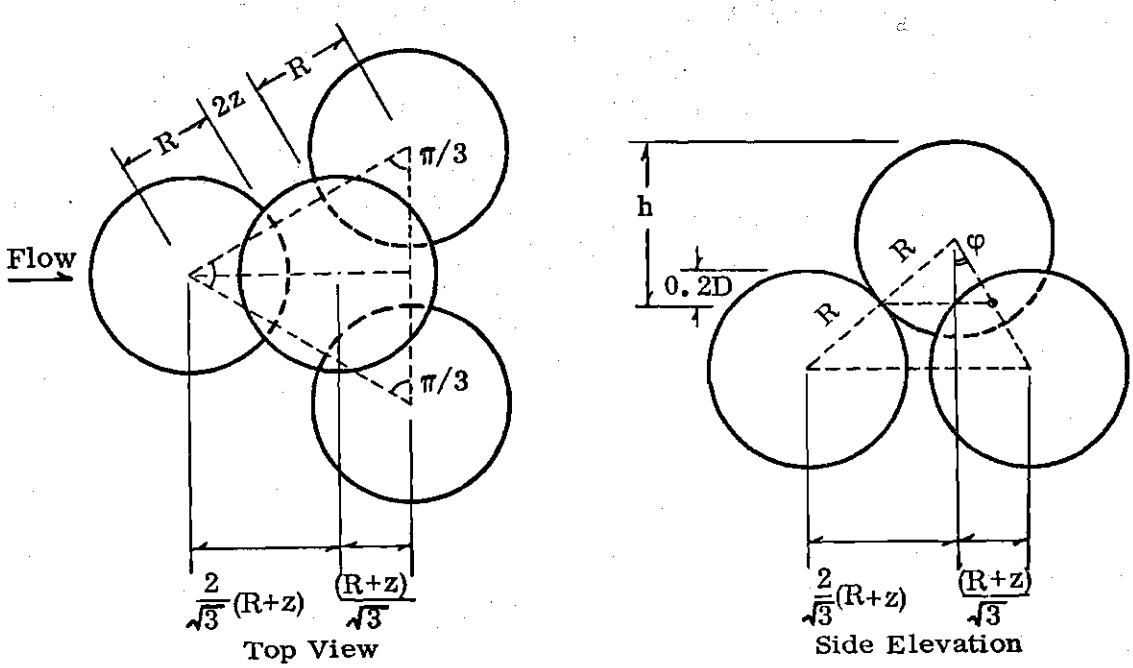

Figure 12. Idealized Bed Particle Arrangement with Uniform Spheres.

The distance from the top of the protruding sphere to the top of the underlying spheres is

$$\frac{R}{\sqrt{3}} \sqrt{3 - (1 + z/R)^2}$$

Assuming the effective wall* being 0.2 D below the top of the underlying spheres, the protrusion condition of the sphere can thus be expressed as

*The effective wall is defined as the origin of the logarithmic velocity distribution. Einstein and El-Samni (10) determined the effective wall as being 0.2 diameter below a plain tangent to the top of the spheres by fitting the logarithmic velocity distribution. Iwagaki and Tsuchiya (15) determined the effective wall as being located 0.25 diameter below the plane tangent to the top layer of the sand particles.

$$\frac{h}{D} = [\,0.2 + \frac{1}{\sqrt{3}} \sqrt{3 - (1 + z/R)^2}\,] \qquad (39)$$

For a value of φ equal to 30 degrees, the corresponding value of z/R is approximately 0.3. The associated protrusion condition, h/D, is then approximately 85 per cent. The fluid-driving moment coefficient, C_I, and the impulsive moment coefficient, C_δ, as obtained from Figures 5 and 11 are 0.68 and 0.32, respectively. Using a momentum correction coefficient, ζ, equal to 0.787 as obtained from Run III-1 of the present study, the critical bottom velocity corresponding to the final stage of the transition can be evaluated. The bottom velocity, u_T, as computed from Equation (24), is 0.87 ft/sec. The corresponding mean velocity, V, obtained from Equations (33) and (34) with u = 0.87 ft/sec at y = 0.85 D, is 2.08 ft/sec.

6. Summary

The critical velocities as determined by different approaches are summarized in Table 3.

Table 3. Summary of Critical Velocities Based on Various Methods

	Method Used By				
	Shields	Mavis	Neill	Carstens	Author
Mean Velocity V(ft/sec)	3.40	2.38*	1.78	3.16	2.08

*The mean velocity is computed based upon the assumption that the bottom velocity is taken at y = D.

CHAPTER V

CONCLUSIONS

1. A simple experimental method has been developed, based upon the proposition of Equation (6), using the weight-restoring moment of the sphere as a gauge to determine the probability distribution of the fluid-driving moment. The method is presently limited to the determination of the high levels of the fluctuating moment. If the response-excitation relationship of the sphere-pin system can be better established, the method could be extended to cover the determination of the lower level moment components. The fluid-driving force pattern associated with the driving moment can be evaluated by the use of Equations (10) and (11). With minor modifications, the method developed for determining the fluid-dynamic moment and forces on a protruding sphere can also be used to determine the fluid-dynamic moment and forces upon other body configurations. The author believes that the development of this simple experimental method is the most important contribution of the study.

2. Variations of the experimentally determined coefficients of moments and forces with the protrusion conditions are shown in Figures 8 and 11. The ratio of the coefficient of lift to drag, C_L^*/C_D^*, decreases from approximately 1.6 to 0.4 as protrusion condition, h/D, increases from 25 per cent to 100 per cent. For h/D equal to or less than 75 per cent, the resultant fluid-driving force can be considered as passing through the centroid of the sphere.

3. There is a transition through which the sphere is removed from a stationary state to an entrainment state. The transition is characterized by the random rocking motion of the sphere. Generalized formulas defining the conditions of the initial stage and the final stage of the transition are given by Equations (14) and (24), respectively. As shown in Figure 10, the range of the differences in the parameter, N_s, between the initial stage and the final stage is rather narrow in comparison with the values of N_s. The effect of non-uniform approach velocity distribution is incorporated in the formulation of Equations (14) and (24) by introducing a momentum correction coefficient, ζ, as defined by Equation (30). However, the reader is cautioned that the value of η was determined by only one experiment with 75 per cent sphere protrusion and with one non-uniform approach velocity distribution.

4. A comparison of the critical velocities for the removal of a sediment particle as determined by various methods are summarized in Table 3. Despite the idealization of the present model, the resulting critical velocity is in close agreement with the critical velocities determined by other methods derived from experiments of natural sediment in water flow. The comparison of the results reassures the validity of the present finding to practical applications. Also, the close agreement of the results indicates that such factors as the added moment of inertia and particle shape play a secondary role in the process of particle removal.

APPENDICES

APPENDIX A

RESPONSE-EXCITATION RELATIONSHIP OF THE SPHERE-PIN SYSTEM

The small angular displacement of the sphere subject to impulsive loads can be obtained by solving the linearized differential equation of angular motion, Equation (5), with the right hand side replaced by an idealized impulsive moment. In order to simplify the analysis, the net impulsive moment is idealized as a positive rectangular impulsive moment followed by a constant negative moment. The duration of the positive moment is considered to be t_0. The ratio of the magnitude of the negative moment to that of the positive moment is m. Neglecting the damping moment in Equation (5), the equation of motion of the system is

$$I\ddot{\theta} - (Wr \sin \theta_s)\,\theta = M[\,U(t) - (m + 1)\,U(t - t_0)\,] \qquad (A.1)$$

in which, M is a constant relating to the magnitude of the net impulsive moment, and $U(t - t_0)$ is the unit step function defined by

$$U(t - t_0) \begin{cases} = 0 & t < t_0 \\ = 1 & t > t_0 \end{cases} \qquad (A.2)$$

Dividing Equation (A.1) by the virtual moment of inertia, I, and designating $a^2 = Wr \sin \theta_s / I$,

$$\ddot{\theta} - a^2\theta = (M/I)[U(t) - (m + 1)\,U(t - t_0)\,] \qquad (A.3)$$

Introducing the dimensionless quantities

$$\underline{t} = t/t_0; \tag{A.4}$$

and

$$\underline{\theta} = (a^2 I/M)\theta \tag{A.5}$$

Equation (A.3) becomes

$$\ddot{\underline{\theta}} - a^2 t_0^2 \underline{\theta} = a^2 t_0^2 [U(\underline{t}) - (m+1)U(\underline{t} - 1)] \tag{A.6}$$

in which $\ddot{\underline{\theta}} = d^2\underline{\theta}/d\underline{t}^2$.

Assuming rest conditions,

$$\underline{\theta}(0) = 0, \ \dot{\underline{\theta}}(0) = 0 , \tag{A.7}$$

The solution of Equation (A.6) can be obtained by the method of Laplace transform. The Laplace transform of the left side of Equation (A.6) subject to the initial values of θ and $\dot{\theta}$ as given by Equation (A.7) is

$$L\{\ddot{\underline{\theta}} - a^2 t_0^2 \underline{\theta}\} = (s^2 - a^2 t_0^2)\, \Theta(s) \tag{A.8}$$

The Laplace transform of the right side of Equation (A.6) is

$$L\{a^2 t_0^2 [U(\underline{t}) - (m+1)\, U(\underline{t} - 1)]\} = a^2 t_0^2 \left(\frac{1}{s} - \frac{m+1}{s} e^{-s}\right) \tag{A.9}$$

Equating Equations (A.8) and (A.9),

$$\Theta(s) = \frac{a^2 t_0^2}{s(s^2 - a^2 t_0^2)} \quad [1 - (m+1)\, e^{-s}] \tag{A.10}$$

By partial fraction, the above equation becomes

$$\Theta(s) = \left(\frac{s}{s^2 - a^2 t_0^2} - \frac{1}{s}\right)\left[1 - (m+1)\, e^{-s}\right] \qquad \text{(A.11)}$$

Hence $\underline{\theta}(\underline{t})$, the inverse transform of $\Theta(s)$, equals

$$\underline{\theta}(\underline{t}) = (\cosh at_0 \underline{t} - 1) - (m+1)\left[\cosh at_0 (\underline{t} - 1) - 1\right] \quad U(\underline{t} - 1) \qquad \text{(A.12)}$$

Equation (A.12) is the response of the sphere in dimensionless form. The response, $\underline{\theta}(\underline{t})$, is characterized by the parameter, at_0, and the moment ratio, m.

Typical response-excitation relationships of the sphere-pin system, with $at_0 = 1$, are shown in Figure A.1. The excursion times (the time interval between the time of take-off and the time of roll-back) of the sphere, t_e, are tabulated in Table A.1 in terms of the ratio, t_e/t_0.

Table A.1. Excursion Time of the Sphere
(t_e/t_0)

m \ at_0	0.5	1.0	1.5	2.0	2.5	3.0
2	2.50	3.60	*	*	*	*
5	1.72	1.83	2.20	*	*	*
10	1.44	1.49	1.58	1.80	*	*
15	1.34	1.36	1.41	1.52	1.80	*
20	1.28	1.30	1.34	1.40	1.54	2.25

*Response, $\underline{\theta}(\underline{t})$, increases monotonically with time, $\underline{t}$.

In Table A.1, limiting values of the excursion time are shown. The blank spaces in the upper right of Table A.1 indicate that the sphere would roll over the pins without falling back to the base for these values of at_0 and m.

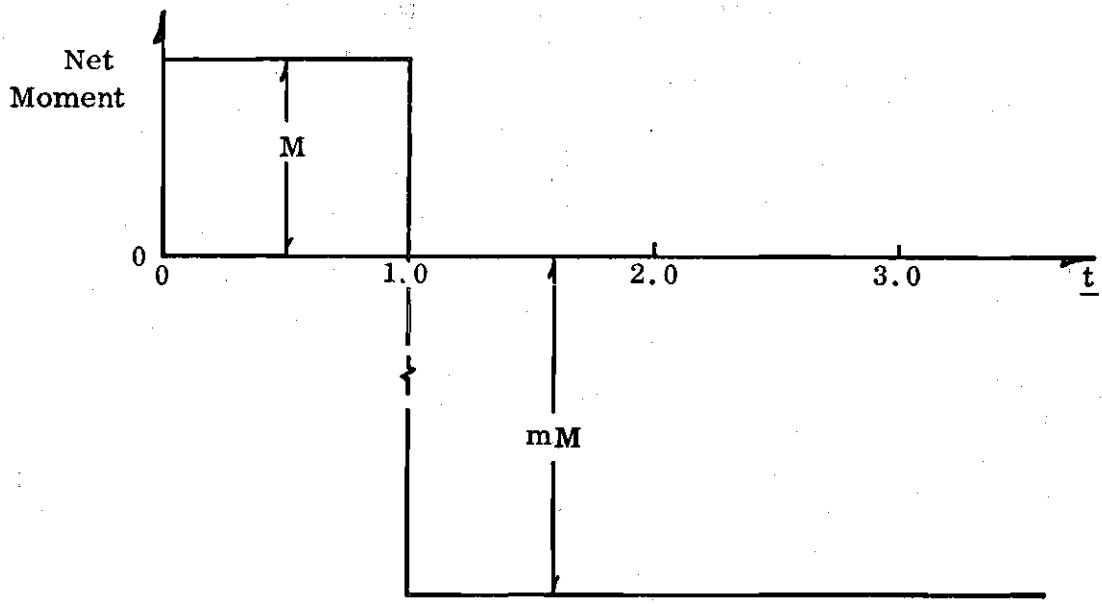

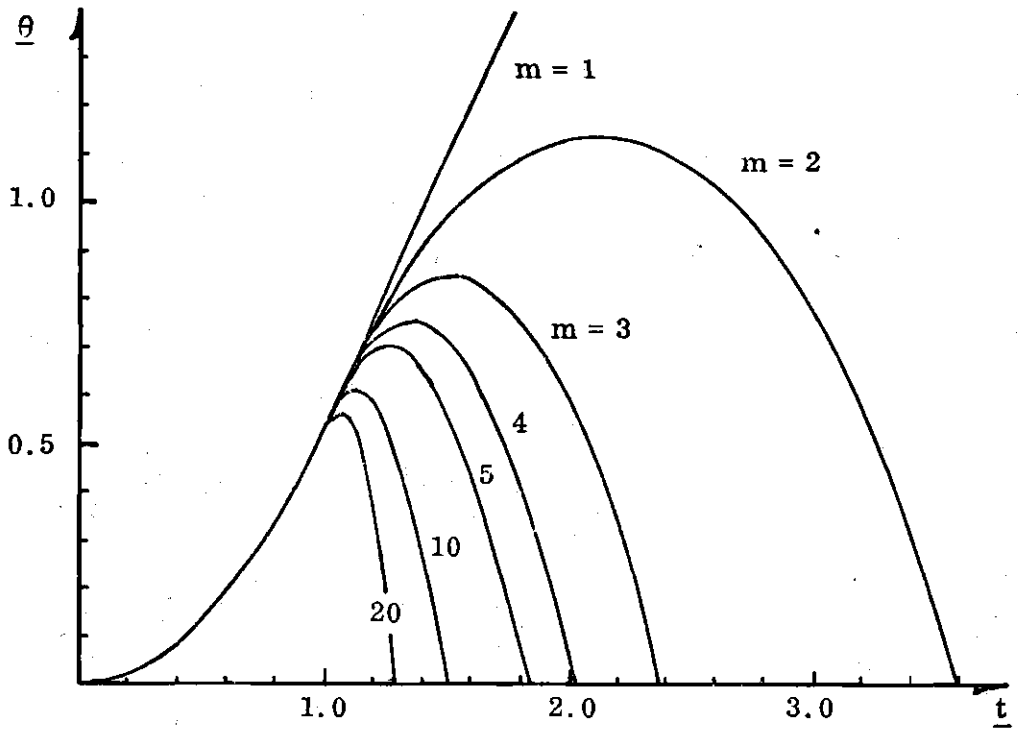

Figure A.1. Response-Excitation Relationship.

APPENDIX B

EXPERIMENTAL RESULTS

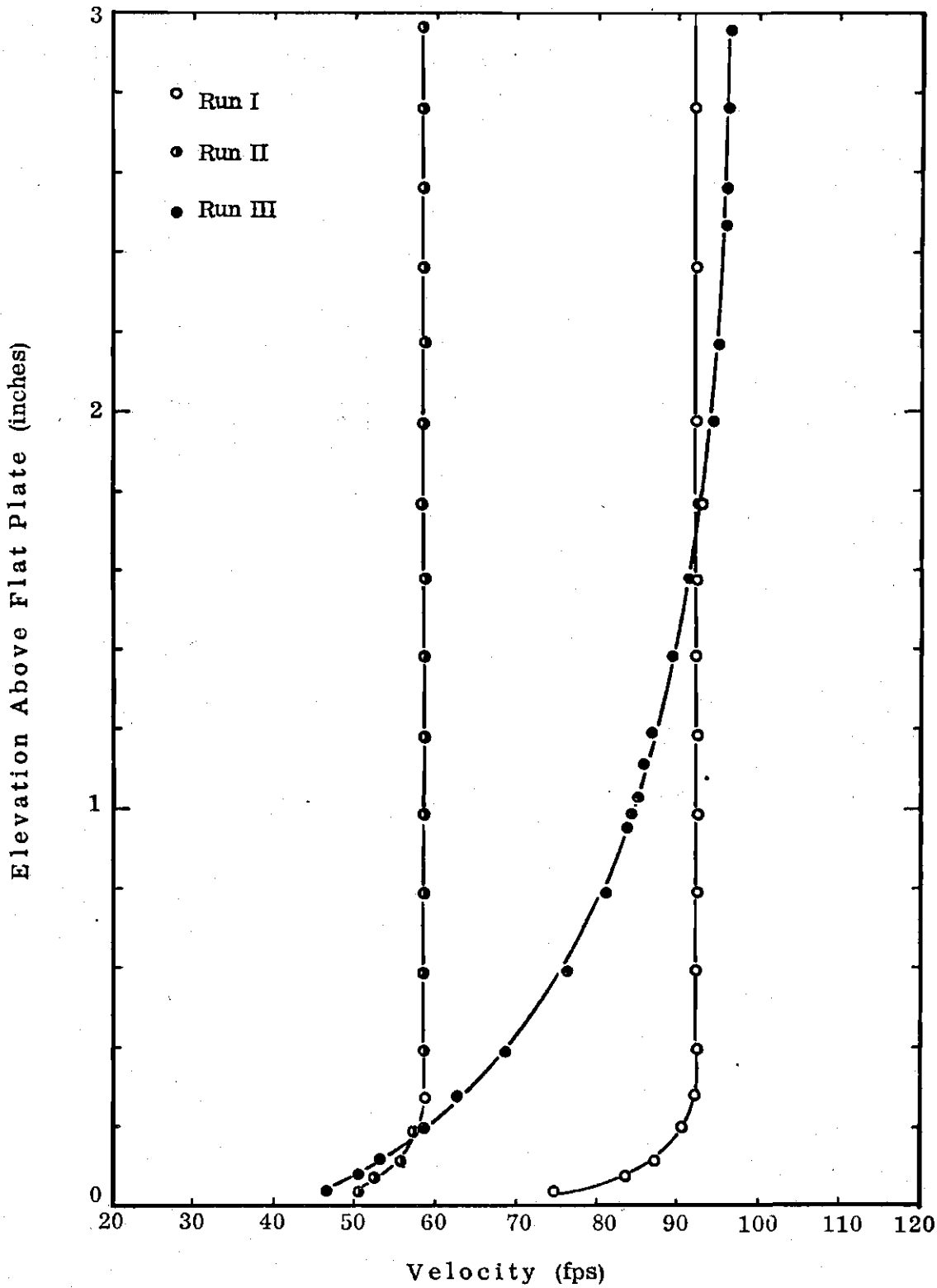

Figure B.1. Approach Velocity Profiles.

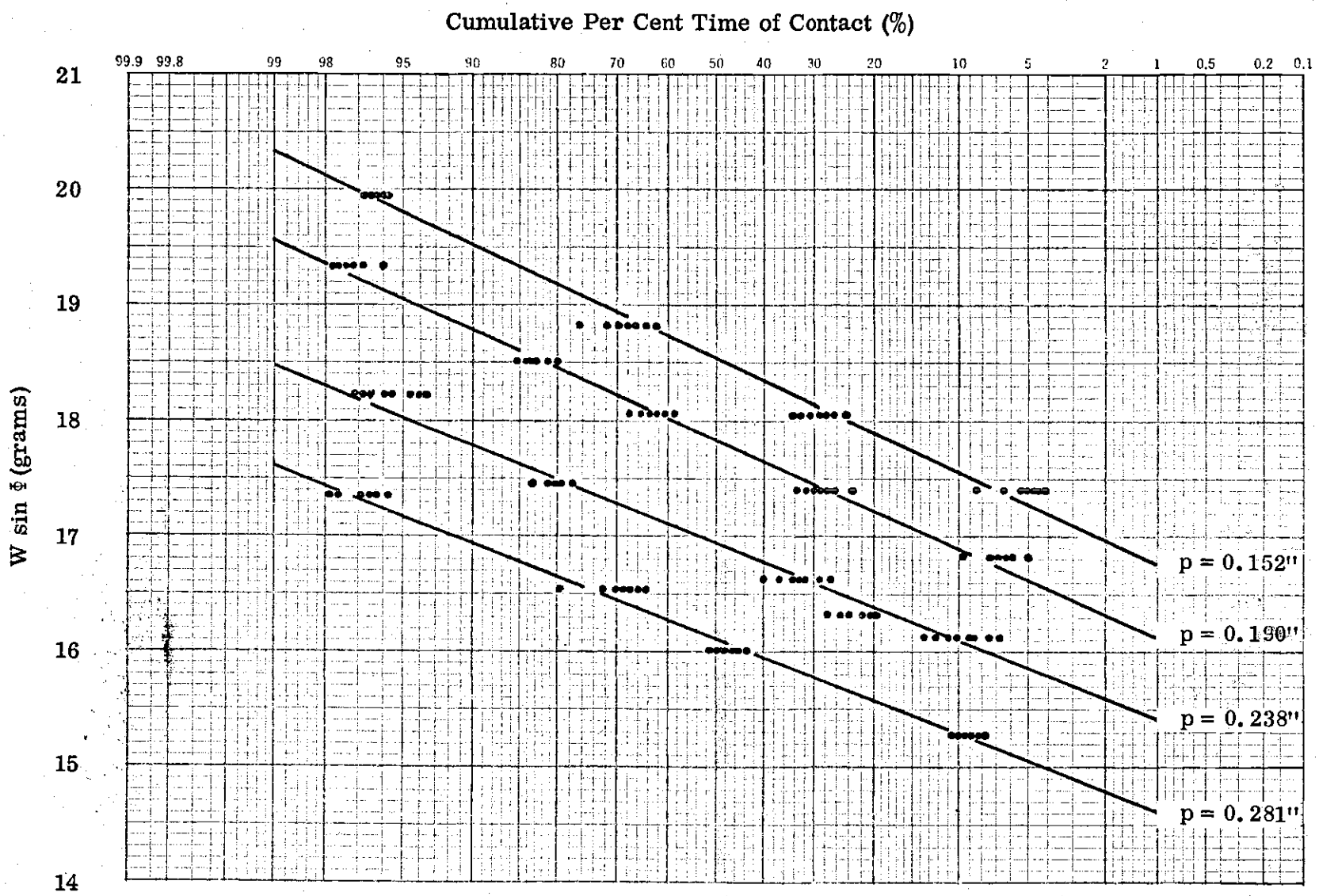

Figure B.2.a. Data of Contact Duration at 100% Protrusion (Run I-8).

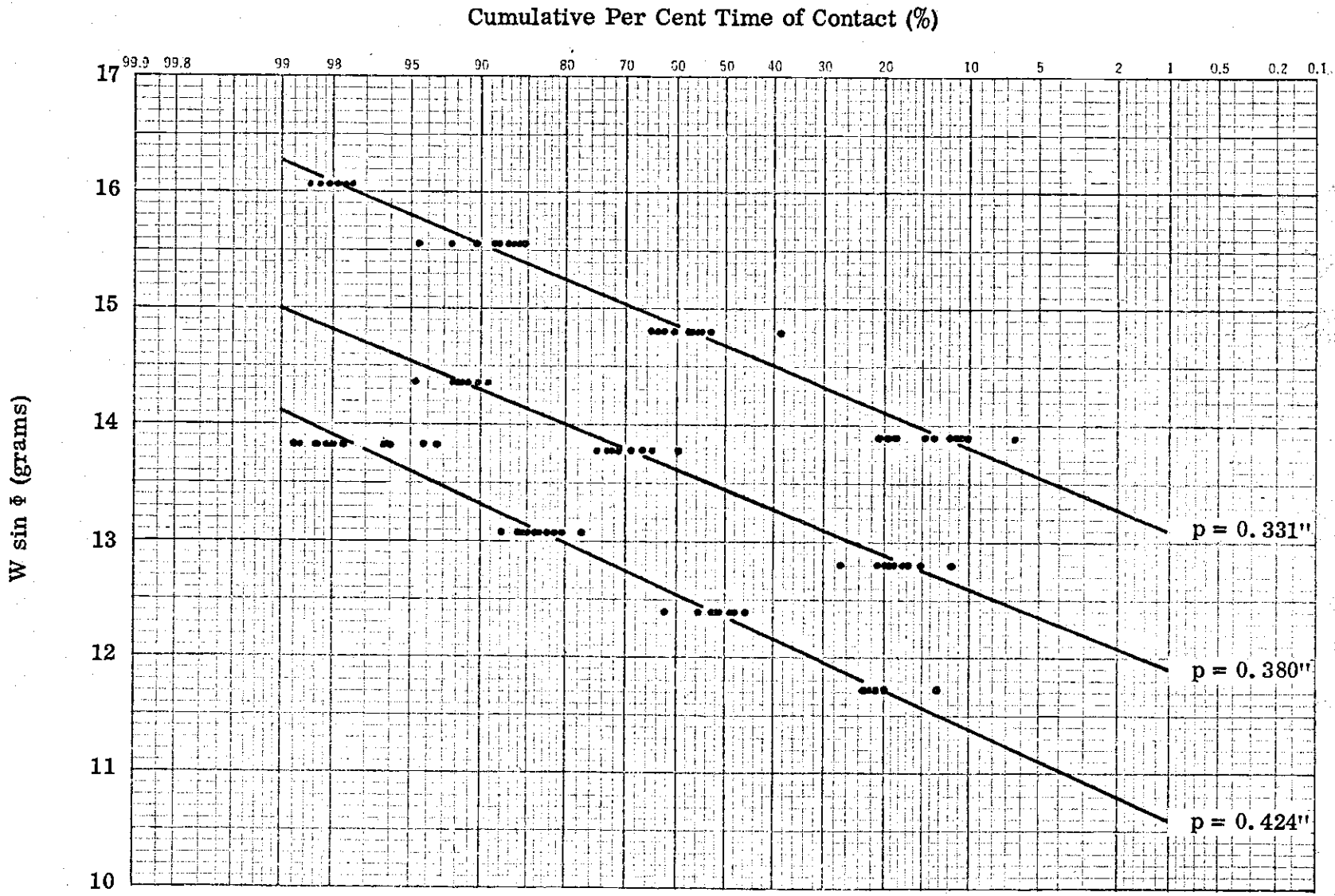

Figure B.2.b. Data of Contact Duration at 100% Protrusion (Run I-8).

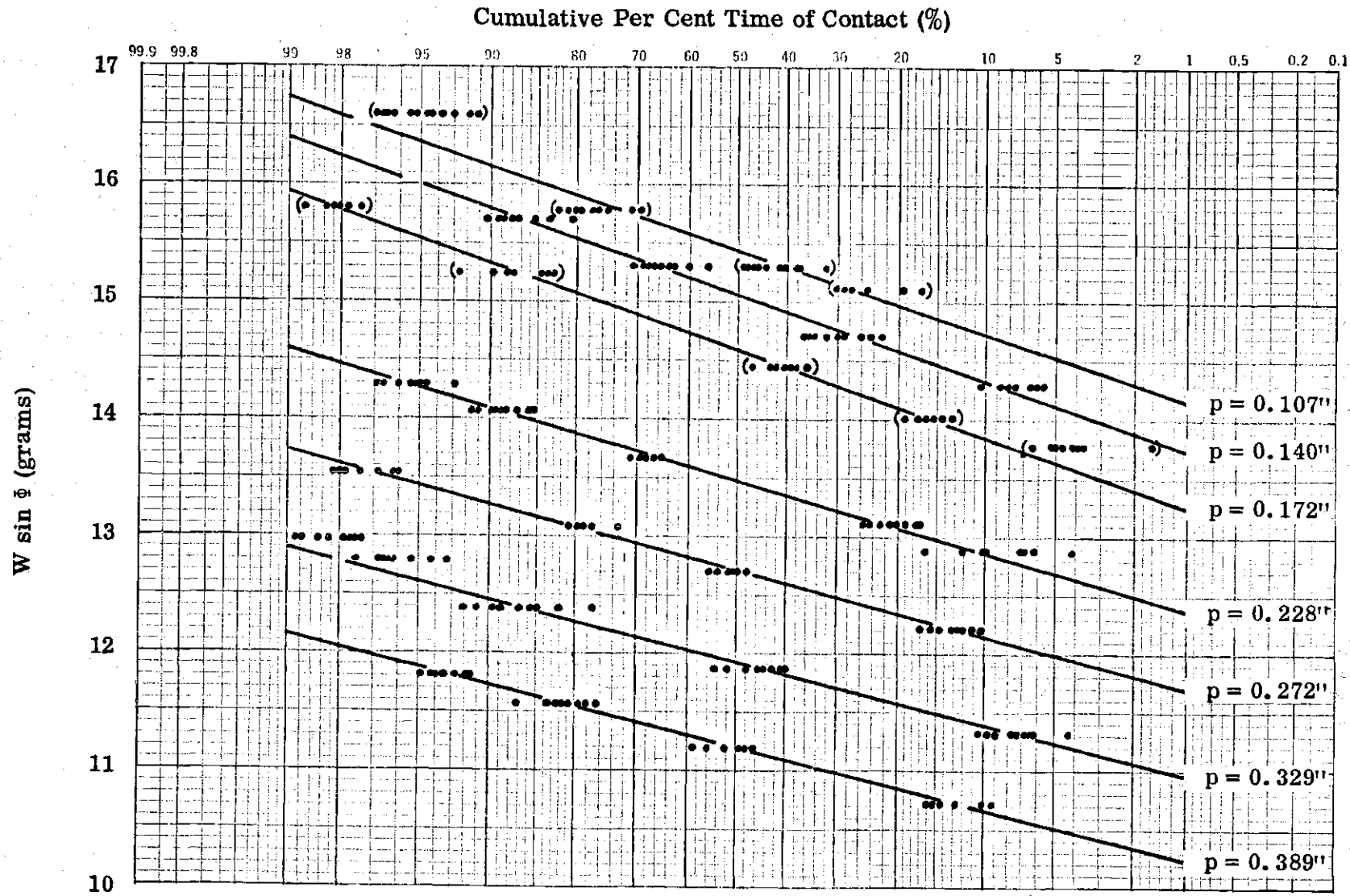

Figure B.3. Data of Contact Duration at 85% Protrusion (Run I-7).

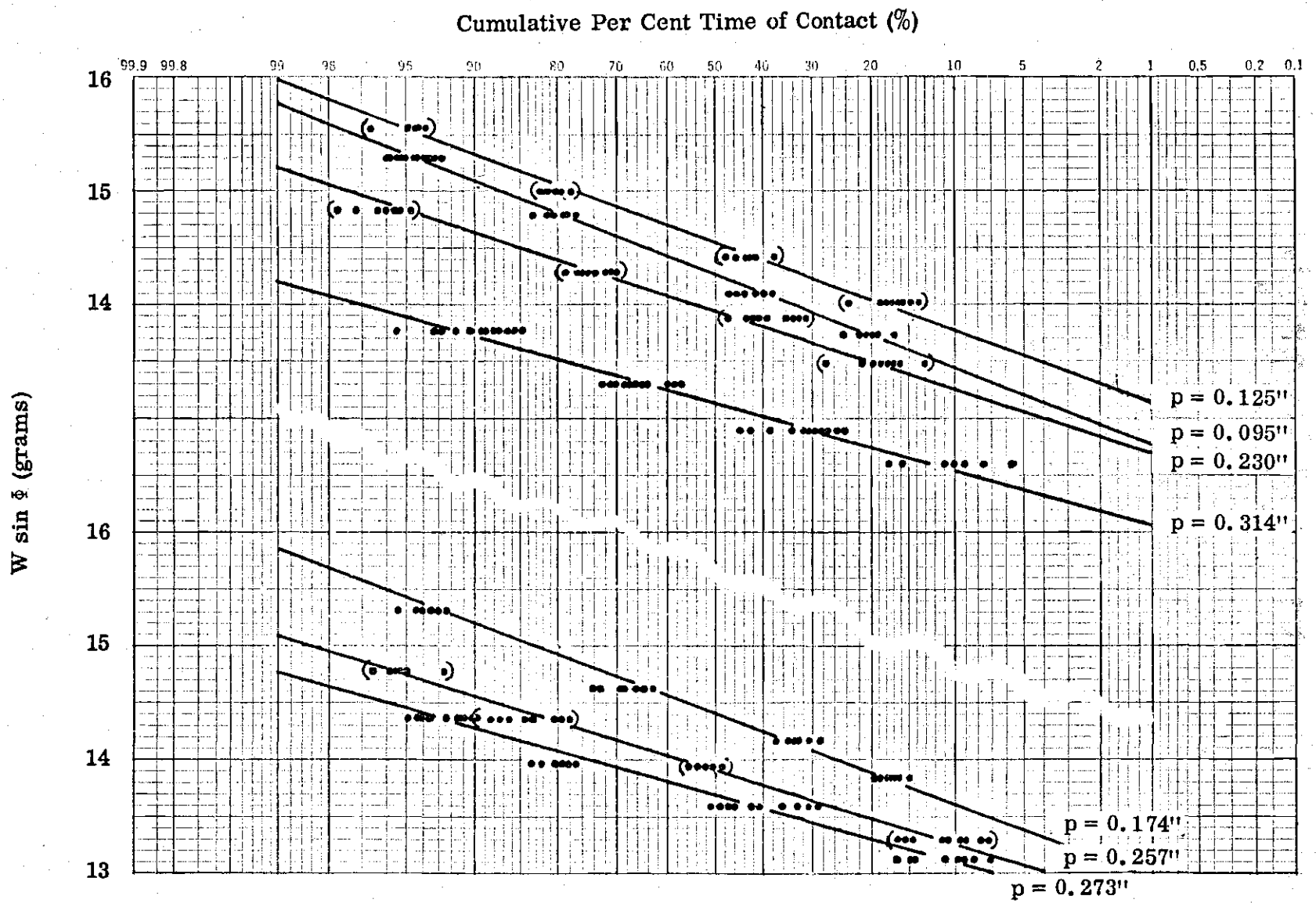

Figure B.4. Data of Contact Duration at 75% Protrusion (Run I-9).

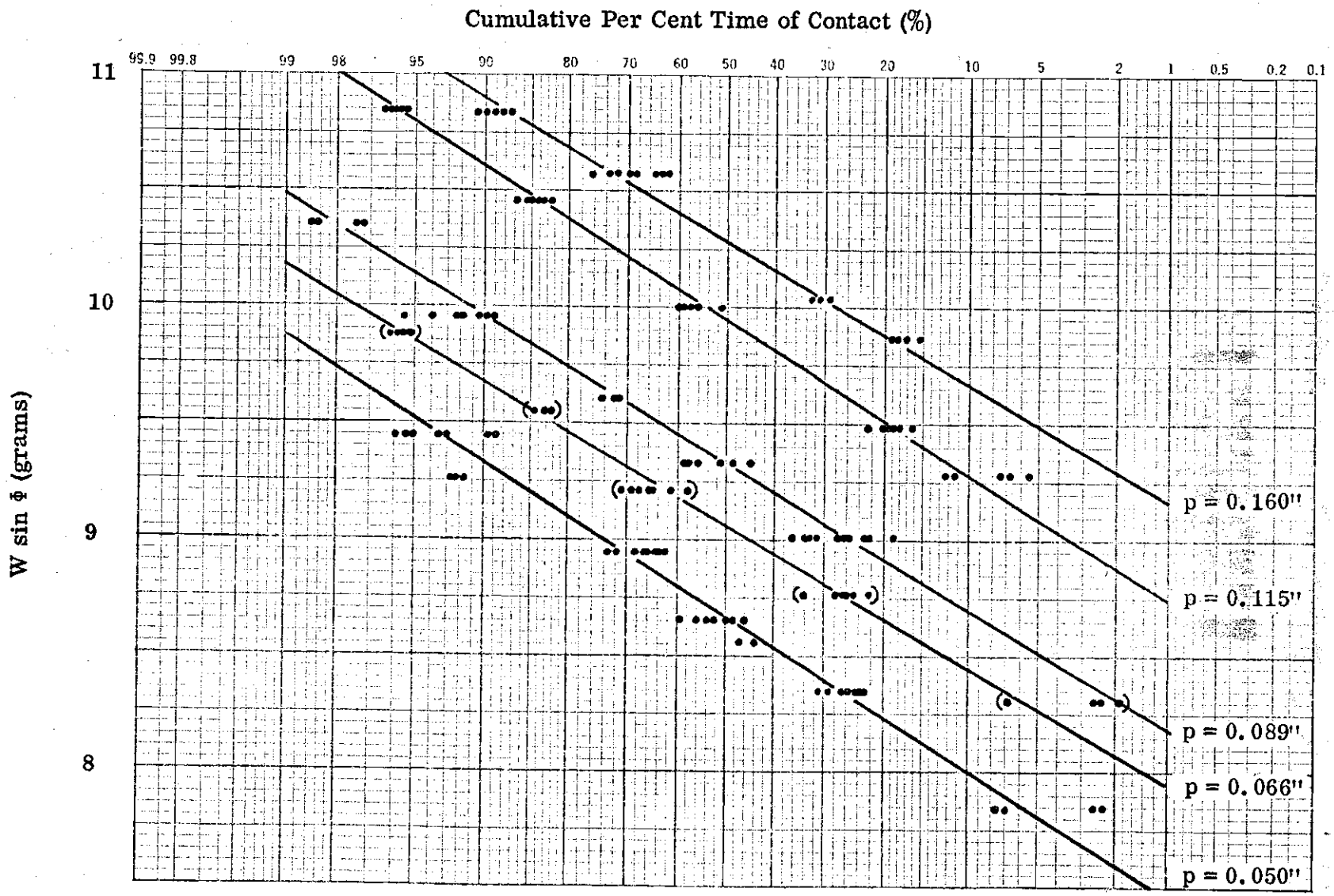

Figure B.5.a. Data of Contact Duration at 50% Protrusion (Run I-4).

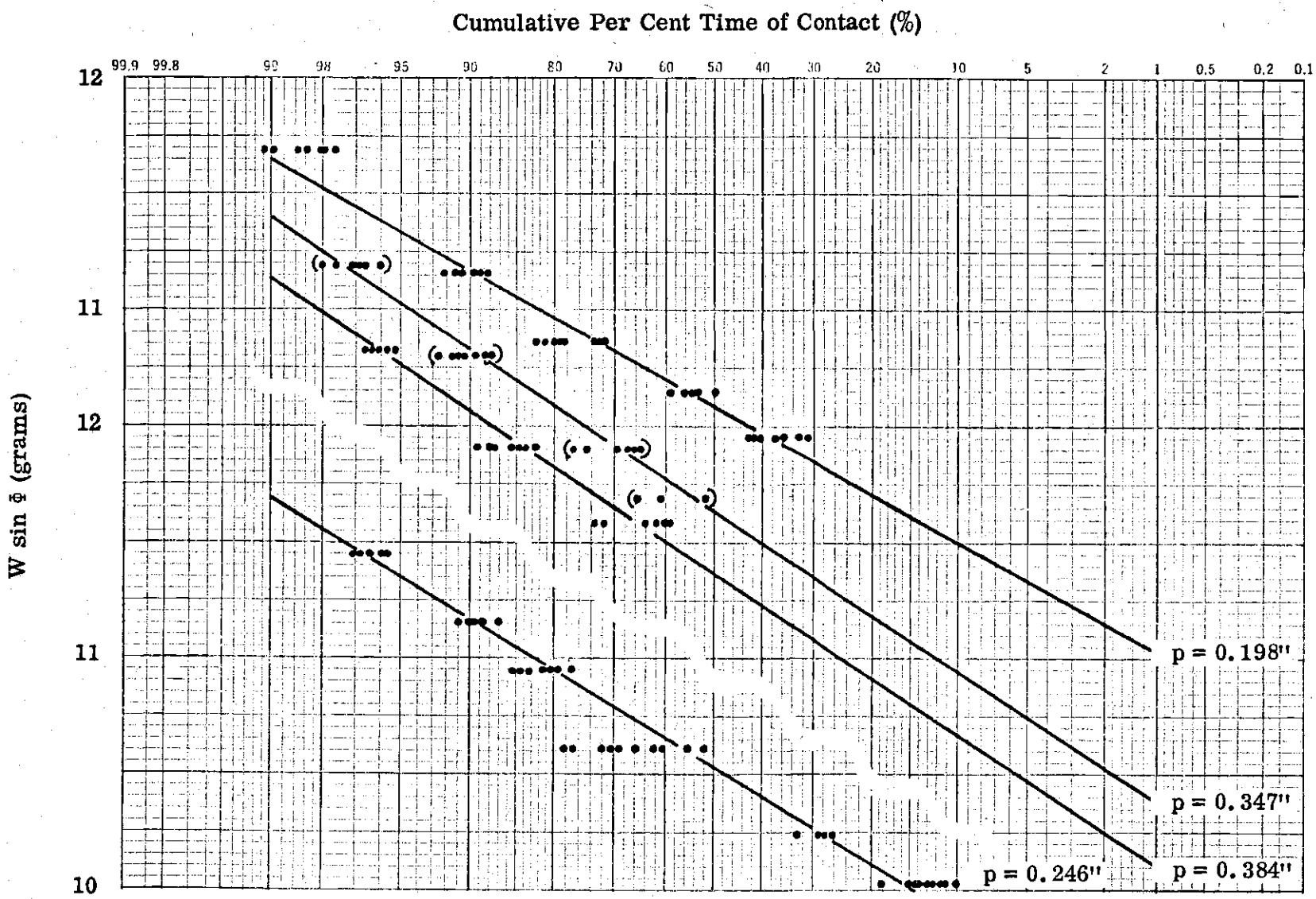

Figure B.5.b. Data of Contact Duration at 50% Protrusion (Run I-4).

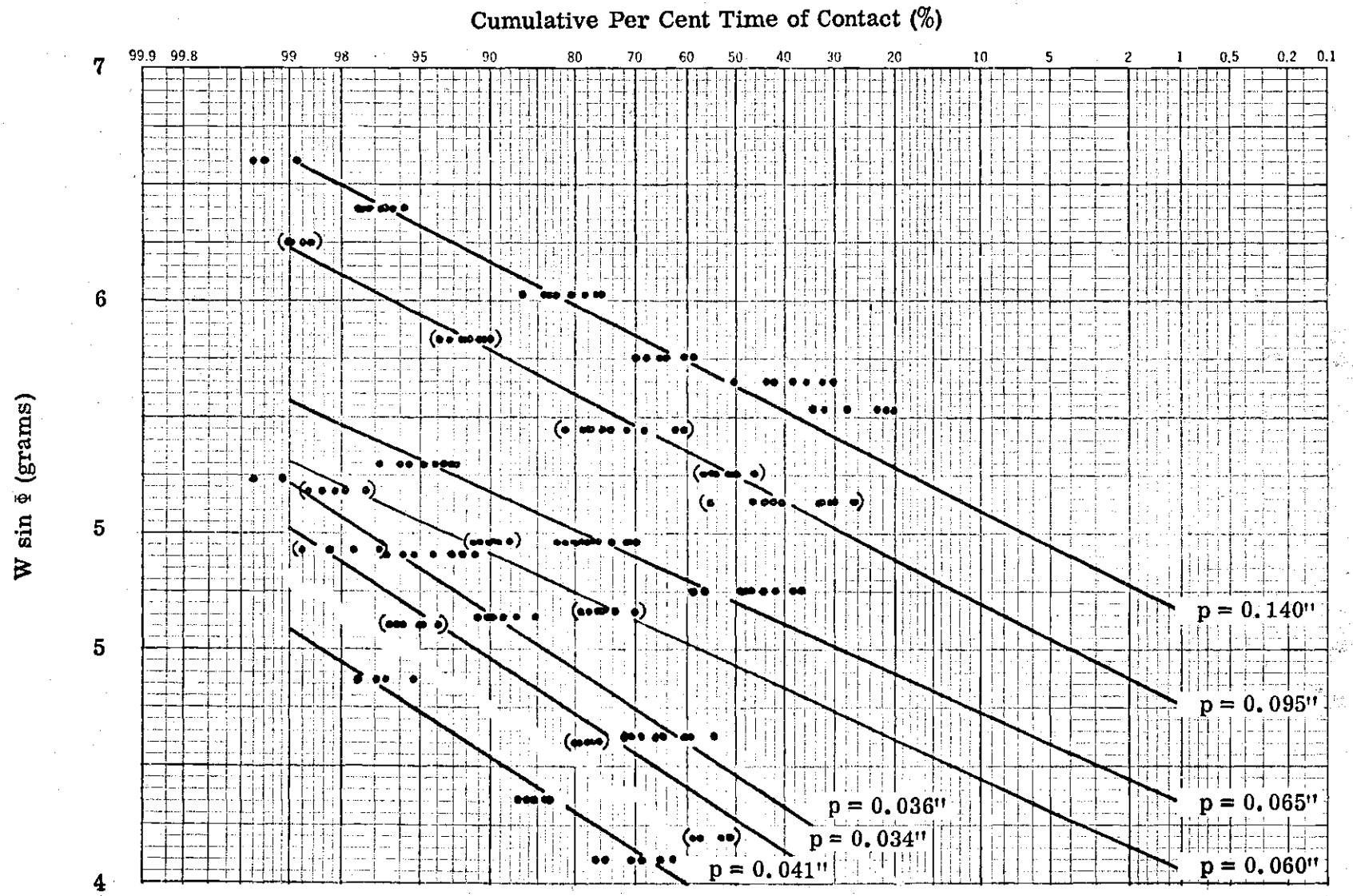

Figure B. 6. a. Data of Contact Duration at 25 % Protrusion (Run I-5).

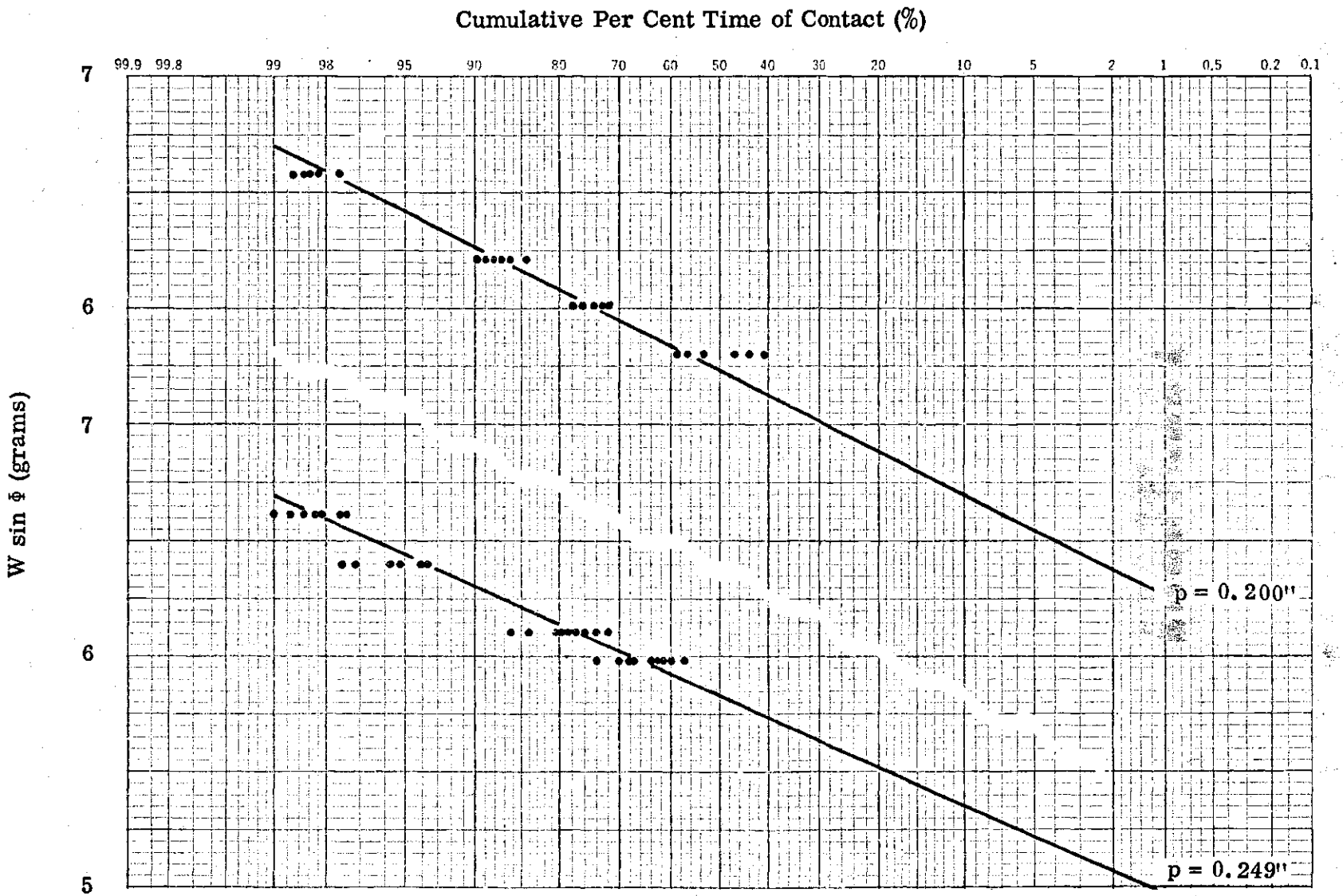

Figure B.6.b. Data of Contact Duration at 25% Protrusion (Run I-5).

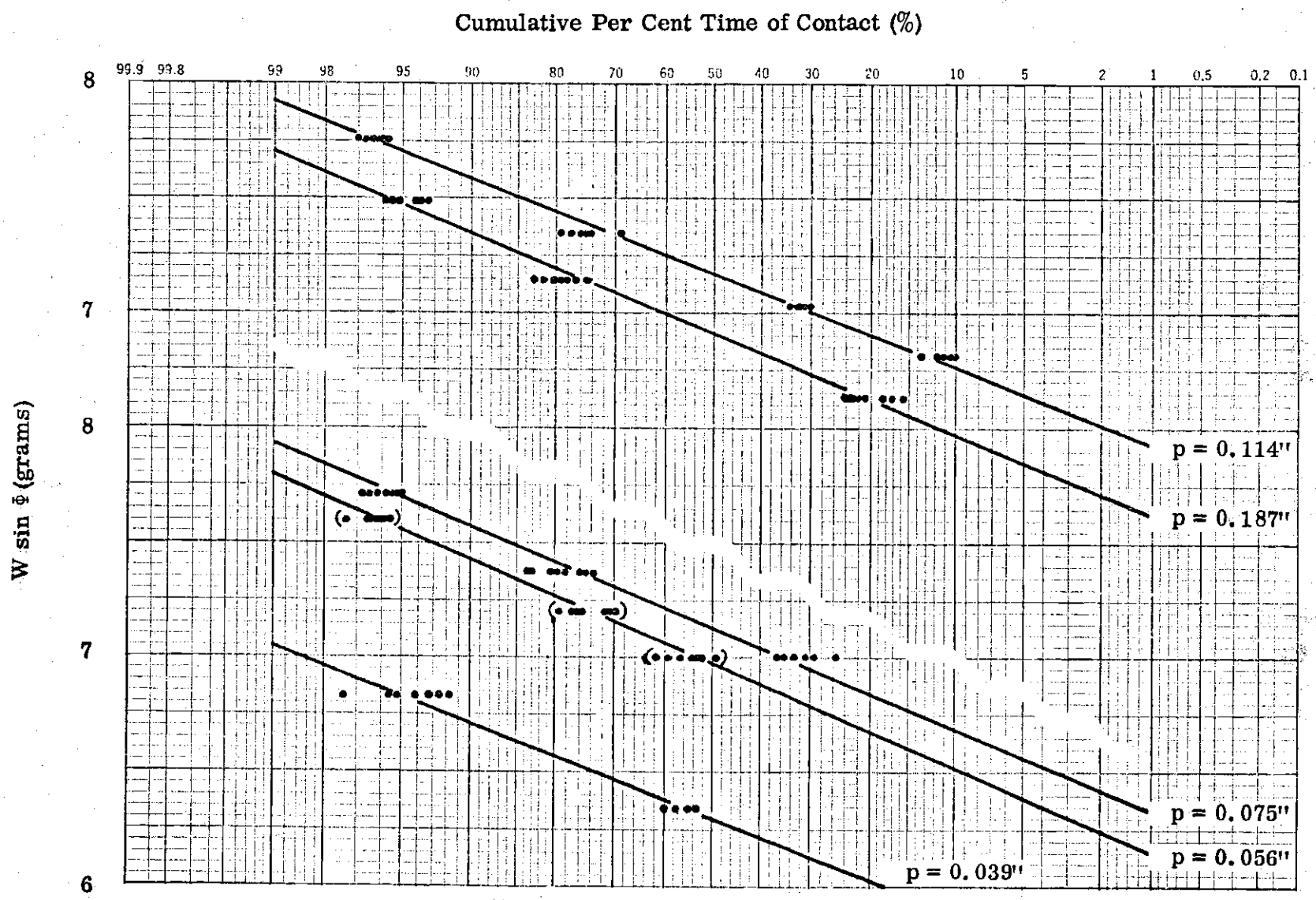

Figure B.7. Data of Contact Duration at 100% Protrusion (Run II-3).

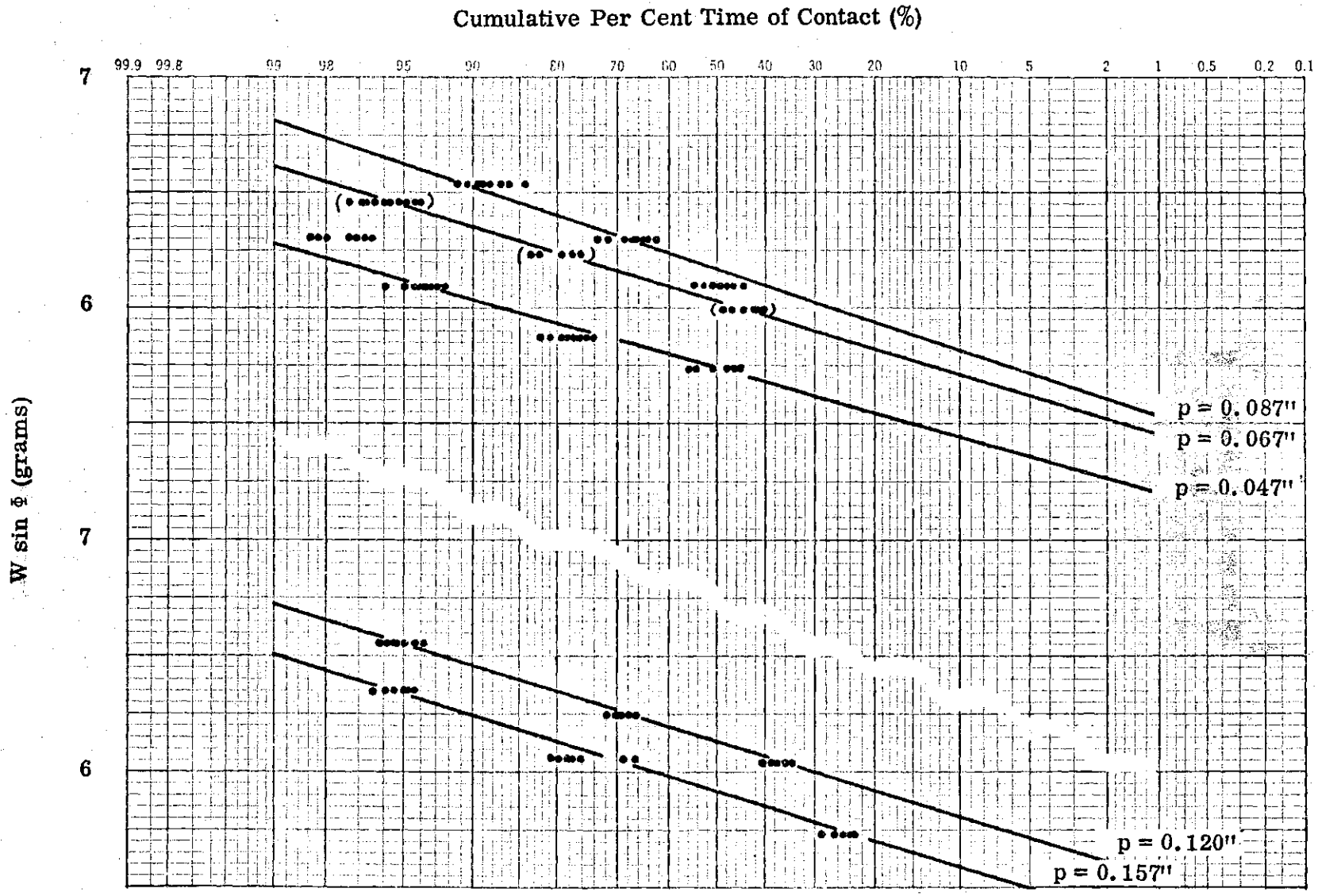

Figure B.8. Data of Contact Duration at 85% Protrusion (Run II-2).

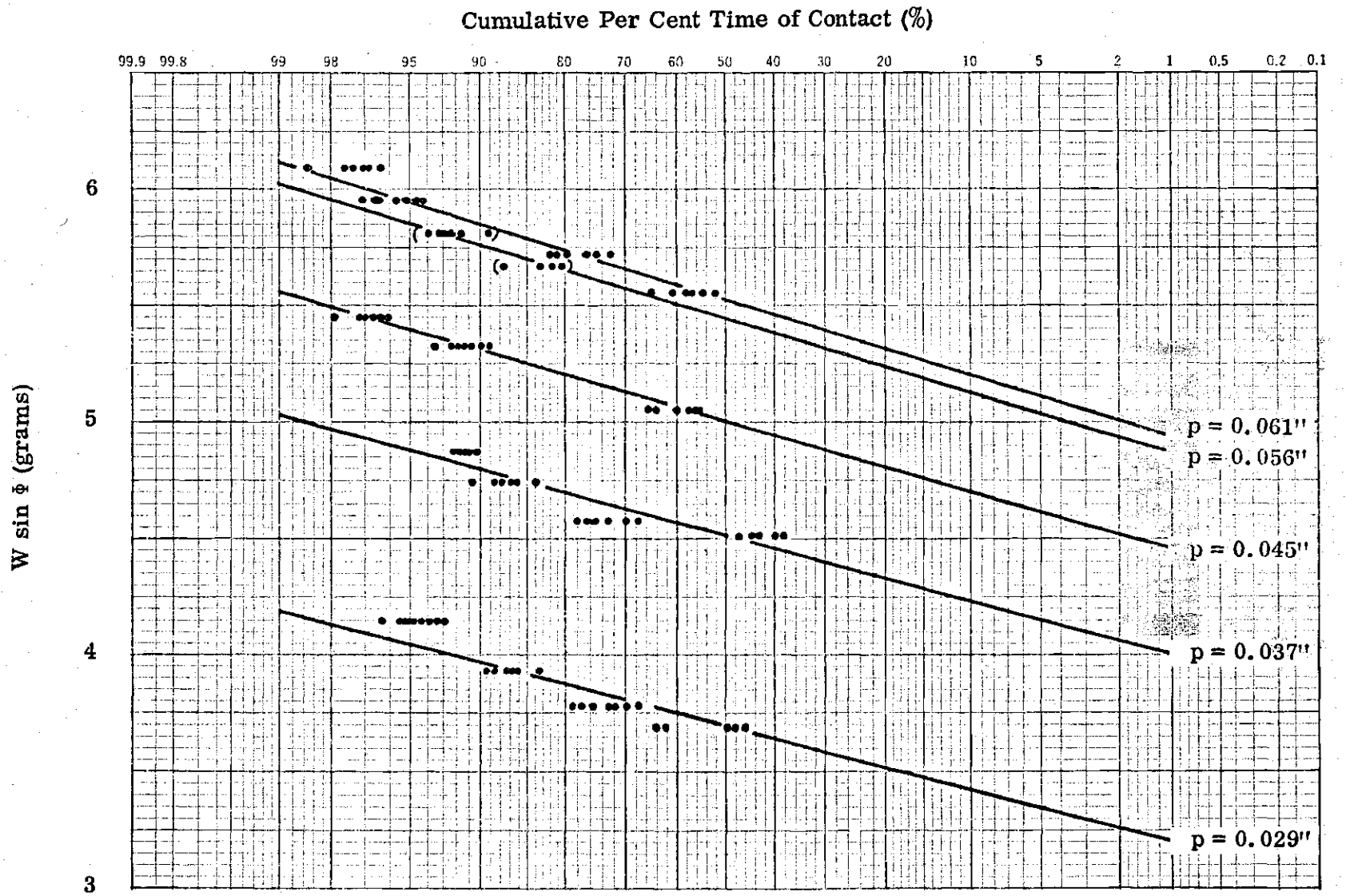

Figure B.9.a. Data of Contact Duration at 75% Protrusion (Run II-1).

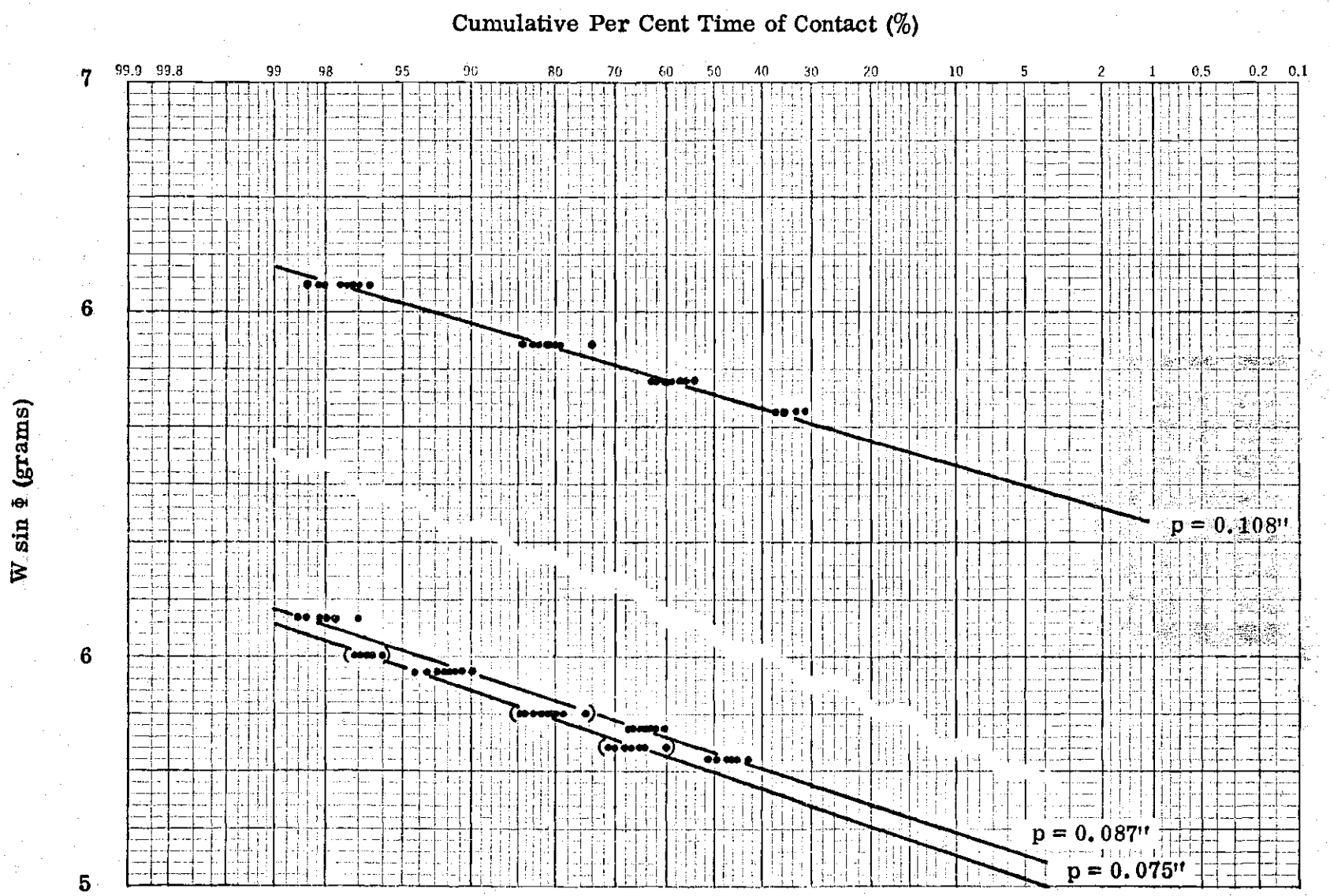

Figure B.9.b. Data of Contact Duration at 75% Protrusion (Run II-1).

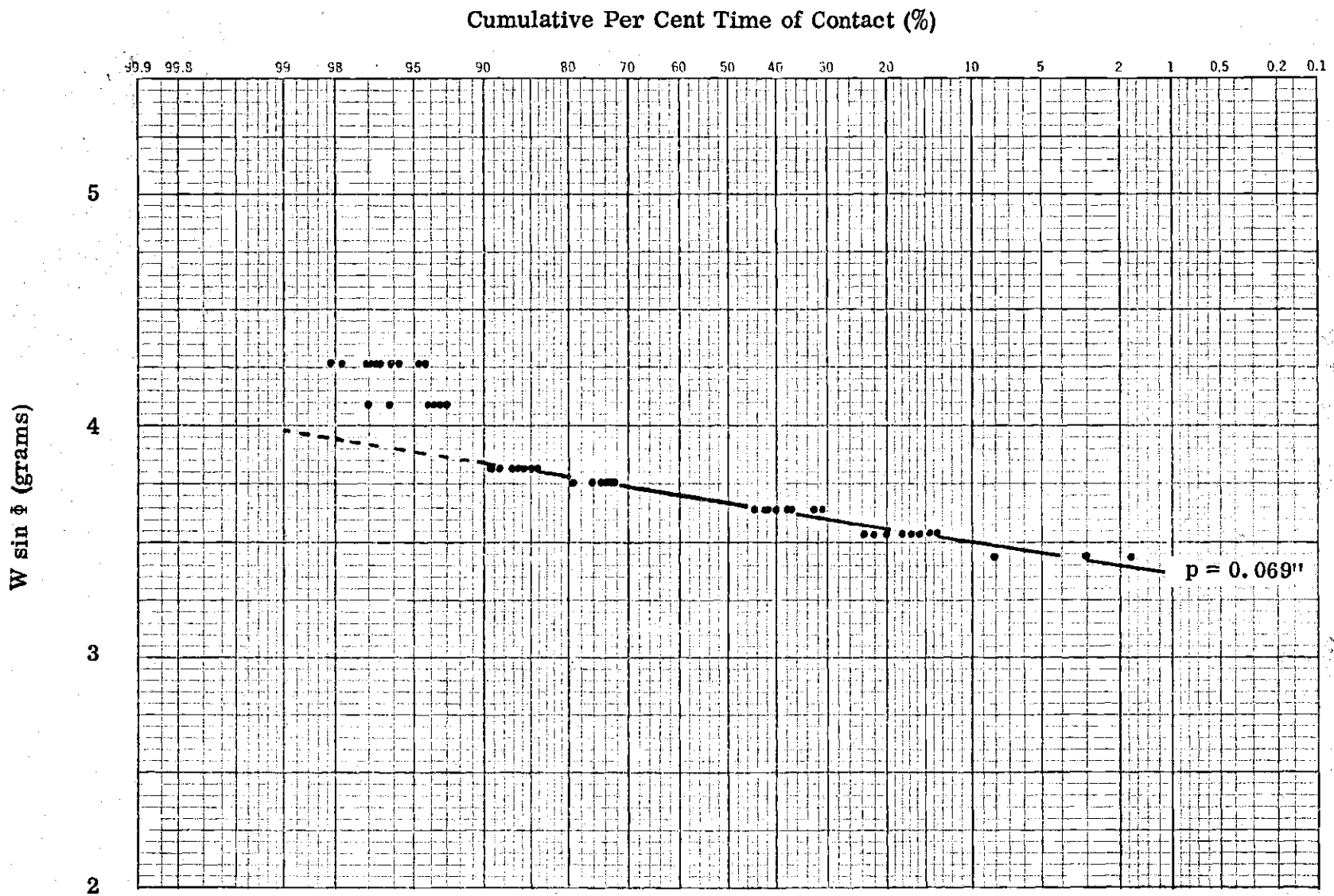

Figure B.10. Data of Contact Duration at 50% Protrusion (Run II-4).

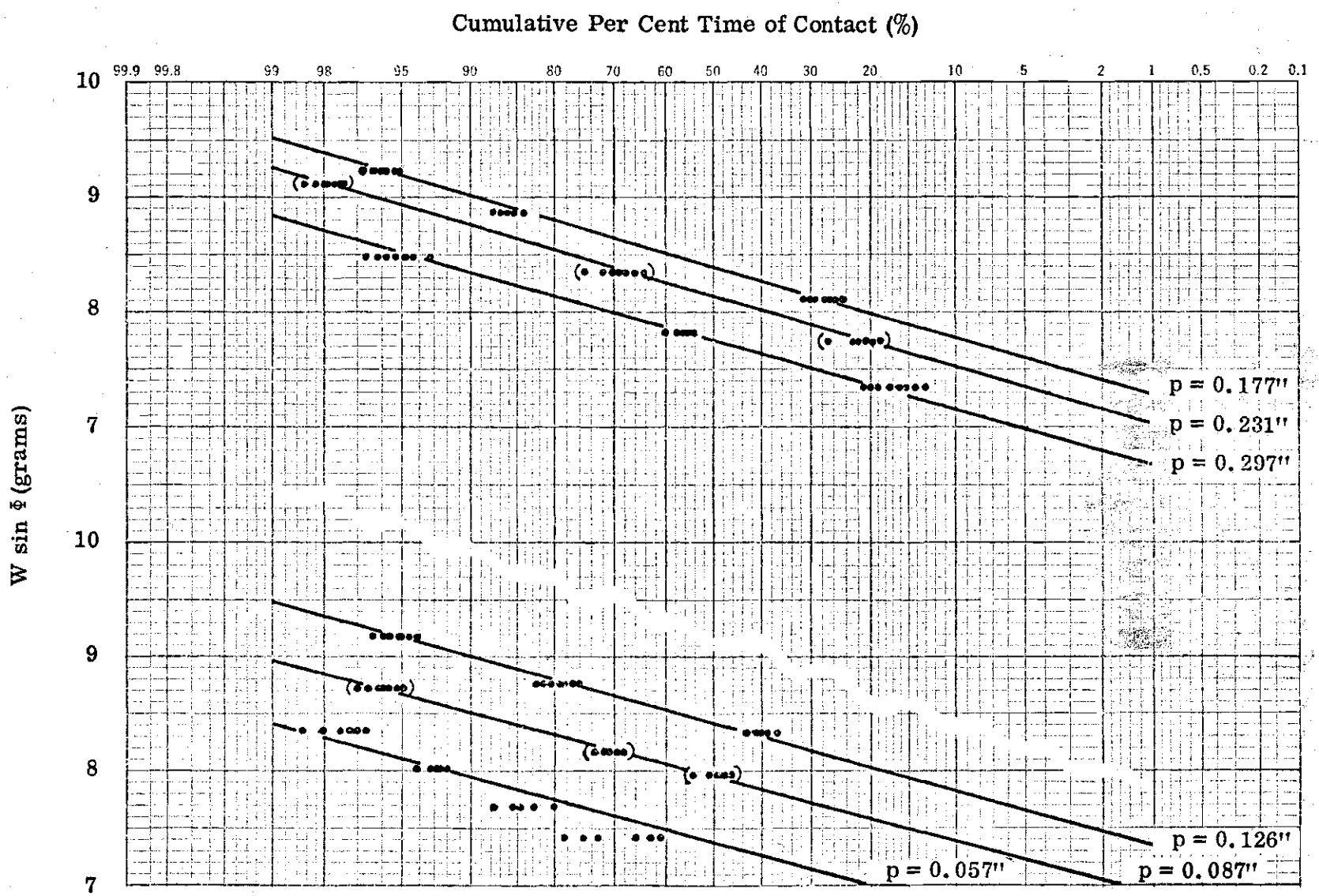

Figure B.11. Data of Contact Duration at 75% Protrusion (Run III-1).

Table B.1. Data of Fluid-Driving Moment Coefficient C_I

Run No.	Protrusion h/D (%)	p (inch)	Φ † (degree)	M_I/r (gram)	C_I ‡
I-8	100	0.152	43.0	19.79	0.812
		0.190	49.3	19.04	0.781
		0.238	56.5	18.01	0.740
		0.281	62.55	17.17	0.705
		0.331	69.2	15.81	0.649
		0.380	75.8	14.55	0.597
		0.424	80.8	13.60	0.558
I-7	85	0.107	34.27	16.35	0.671
		0.140	40.85	16.00	0.657
		0.172	46.40	15.53	0.638
		0.228	55.12	14.26	0.585
		0.272	61.30	13.43	0.552
		0.329	68.94	12.61	0.518
		0.389	76.50	11.88	0.488
I-9	75	0.095	31.6	15.32	0.629
		0.125	38.0	15.55	0.639
		0.174	46.75	15.42	0.633
		0.230	55.4	14.82	0.608
		0.257	59.5	14.72	0.605
		0.273	61.5	14.45	0.593
		0.314	67.0	13.88	0.570
I-4	50	0.050	19.0	9.51	0.390
		0.066	24.1	9.84	0.404
		0.089	30.35	10.14	0.417
		0.115	35.92	10.80	0.443
		0.160	44.4	11.08	0.455
		0.198	50.6	11.33	0.465
		0.347	71.46	11.03	0.453
		0.384	75.9	10.76	0.442
		0.246	57.73	11.35	0.466

Table B.1 (Continued). Data of Fluid-Driving Moment Coefficient C_I

Run No.	Protrusion h/D (%)	p (inch)	$\bar{\Phi}$† (degree)	M_I/r (gram)	C_I‡
I-5	25	0.034	11.48	4.65	0.191
		0.036	12.84	4.85	0.199
		0.041	15.2	4.73	0.194
		0.065	23.8	5.32	0.218
		0.095	31.6	5.93	0.244
		0.140	40.75	6.31	0.259
		0.200	50.9	6.42	0.264
		0.249	58.2	6.44	0.264
II-3	100	0.039	14.08	6.83	0.698
		0.056	20.93	7.56	0.773
		0.075	25.6	7.70	0.787
		0.114	35.8	7.70	0.787
		0.187	50.4	7.47	0.763
II-2	85	0.047	17.62	6.12	0.626
		0.067	24.35	6.45	0.659
		0.087	29.65	6.62	0.677
		0.120	37.0	6.55	0.670
		0.157	43.85	6.33	0.647
II-1	75	0.029	8.1	4.05	0.414
		0.037	12.9	4.88	0.499
		0.045	16.86	5.40	0.552
		0.056	20.9	5.85	0.598
		0.061	22.55	5.94	0.607
		0.075	26.6	5.96	0.610
		0.087	29.55	6.02	0.615
		0.108	34.5	6.04	0.617
II-4	50	0.069	25.0	3.88	0.396
III-1	75	0.057	21.1	8.12	0.566
		0.087	29.65	8.68	0.605
		0.126	38.2	9.18	0.640
		0.177	47.25	9.18	0.640

Table B.1 (Continued). Data of Fluid-Driving Moment Coefficient C_I

Run No.	Protrusion h/D (%)	p (inch)	Φ† (degree)	M_I/r (gram)	C_I‡
		0.231	55.55	8.92	0.622
		0.297	64.73	8.50	0.593

† $\Phi = \arccos (R-p)/(R^2 - w^2)^{\frac{1}{2}}$; R = 0.5 inch, w = 0.155 inch.

‡ $C_I = (M_I/r)/\zeta K$; K = 24.35 grams; ζ = 1.0 for all tests of Run I
K = 9.78 grams; ζ = 1.0 for all tests of Run II
K = 18.22 grams; ζ = 0.787 for Run III-1.

Table B. 2. Data of Impulsive Moment Coefficient C_δ

Run No.	Protrusion h/D (%)	p (inch)	Φ (degree)	$C_I^\dagger$	M_F/r (gram)	$C_F^\ddagger$	W (gram)	C_δ
I-8	100	0.113	35.52		14.81	0.608	25.50	
		0.127	38.35		14.20	0.583	22.92	
		0.154	43.3		13.24	0.543	19.32	
		0.184	48.4	0.785	12.86	0.527	17.20	0.883
		0.210	52.4	0.763	11.77	0.483	14.86	1.04
		0.231	55.5	0.745	10.92	0.448	13.24	1.175
		0.091	30.6		14.90	0.611	29.21	
		0.251	58.4	0.727	10.13	0.416	11.90	1.306
		0.135	39.85		13.66	0.560	21.30	
		0.163	44.85	0.801	13.0	0.533	18.45	0.925
		0.244	57.43	0.733	10.17	0.417	12.065	1.330
		0.265	60.4	0.714	9.17	0.376	10.55	1.55
		0.275	61.8	0.703	9.05	0.372	10.27	1.53
		0.278	62.2	0.700	8.71	0.358	9.855	1.638
		0.283	62.88	0.696	8.76	0.360	9.85	1.592
		0.356	72.4	0.620	6.71	0.276	7.04	2.13
I-7	85	0.090	30.4	0.677	13.78	0.565	27.19	0.383
		0.124	37.8	0.664	13.40	0.550	21.86	0.392
		0.145	41.7	0.653	12.90	0.529	19.39	0.437
		0.187	48.8	0.628	12.05	0.495	16.00	0.489
		0.221	54.1	0.604	11.28	0.463	13.91	0.542
		0.257	59.25	0.577	10.46	0.429	12.17	0.598
		0.282	62.7	0.557	9.80	0.402	11.02	0.658
		0.125	38.0	0.663	13.10	0.537	21.30	0.442
		0.155	43.5	0.648	12.70	0.521	18.45	0.453
		0.256	59.13	0.577	10.35	0.425	12.065	0.622
		0.283	62.87	0.557	9.39	0.386	10.55	0.757
		0.299	65.0	0.543	8.93	0.366	9.855	0.813
		0.299	65.0	0.543	9.31	0.382	10.27	0.711
		0.427	81.2		6.95	0.287	7.04	
I-9	75	0.090	30.5	0.626	13.30	0.546	26.23	0.282
		0.152	43.0	0.640	12.97	0.532	19.01	0.378
		0.193	49.8	0.630	12.50	0.513	16.36	0.413

Table B.2 (Continued). Data of Impulsive Moment Coefficient C_δ

Run No.	Protrusion h/D (%)	p (inch)	Φ (degree)	C_I †	M_F/r (gram)	C_F ‡	W (gram)	C_δ
I-9	75	0.252	58.6	0.605	11.66	0.478	13.67	0.452
		0.074	26.48	0.615	13.16	0.540	29.47	0.271
		0.116	36.10	0.636	13.46	0.552	22.80	0.290
		0.124	37.76	0.639	13.04	0.535	21.30	0.368
		0.158	44.0	0.638	12.82	0.527	18.45	0.392
		0.300	65.12	0.580	10.94	0.449	12.065	0.493
		0.355	72.25	0.540	10.05	0.412	10.55	0.501
		0.406	78.6	0.494	10.07	0.413	10.27	0.302
		0.399	77.7	0.502	9.675	0.397	9.855	0.413
I-4	50	0.042	15.8		7.85	0.322		
		0.055	20.6	0.388	8.51	0.350	24.17	0.214
		0.071	25.5	0.409	8.86	0.364	20.61	0.240
		0.117	36.3	0.444	9.36	0.384	15.81	0.297
		0.135	39.9	0.452	9.79	0.402	15.24	0.234
		0.167	45.55	0.461	9.89	0.406	13.85	0.208
		0.199	50.75	0.465	9.98	0.410	12.89	0.242
		0.262	60.0	0.465	10.06	0.413	11.61	0.218
		0.306	65.9	0.460	10.04	0.412	10.99	0.195
		0.362	73.3	0.445	9.55	0.392	9.99	0.216
		0.067	24.2	0.403	8.75	0.359	21.30	0.239
		0.089	30.3	0.426	9.35	0.384	18.45	0.212
		0.230	55.4	0.467	9.93	0.408	12.065	0.256
		0.294	64.33	0.461	9.525	0.391	10.57	0.303
		0.344	70.85	0.450	9.175	0.377	10.27	0.298
		0.352	71.88	0.448	9.37	0.385	9.855	0.265
		0.368	73.8	0.444	9.46	0.388	9.85	0.231
I-5	25	0.034	11.48	0.191	3.70	0.152	18.61	0.509
		0.039	14.10	0.200	3.82	0.157	15.69	0.530
		0.063	23.20	0.225	4.70	0.193	11.91	0.325
		0.102	33.20	0.249	5.36	0.220	9.80	0.243
		0.131	39.15	0.259	5.47	0.225	8.67	0.285
		0.194	50.0	0.269	5.725	0.235	7.48	0.263
		0.221	54.1	0.270	5.825	0.239	7.19	0.231
		0.062	22.8	0.224	4.57	0.188	11.79	0.376
		0.027	5.74		2.13	0.087	21.30	
		0.035	12.06	0.191	3.86	0.158	18.45	0.440

Table B. 2 (Continued). Data of Impulsive Moment Coefficient C_δ

Run No.	Protrusion h/D (%)	p (inch)	Φ (degree)	C_I †	M_F/r (gram)	C_F ‡	W (gram)	C_δ
I-5	25	0.060	22.3	0.228	4.58	0.188	12.065	0.418
		0.080	28.0	0.237	4.825	0.198	10.27	0.382
		0.081	28.2	0.238	4.66	0.191	9.855	0.476
		0.085	29.2	0.240	4.81	0.197	9.85	0.422
		0.232	55.7	0.270	5.385	0.221	6.52	0.392
II-3	100	0.037	12.83		6.235	0.638	28.05	
		0.054	20.36		6.825	0.697	19.61	
		0.062	22.8		6.67	0.682	17.22	
		0.085	29.2		6.49	0.664	13.28	
		0.125	37.9	0.823	5.97	0.610	9.72	0.662
		0.178	47.35	0.790	5.22	0.533	7.09	0.882
		0.047	17.63		6.46	0.660	21.30	
		0.055	20.6		6.49	0.664	18.45	
		0.093	31.15		6.24	0.638	12.065	
		0.116	36.2		6.065	0.620	10.27	
		0.190	49.3	0.782	4.94	0.505	6.52	0.988
II-2	85	0.044	16.49		5.50	0.562	19.40	
		0.065	23.80		5.87	0.600	14.53	
		0.074	26.30		5.85	0.598	13.20	
		0.081	28.20		5.82	0.595	12.31	
		0.107	34.2	0.672	5.62	0.578	10.04	0.311
		0.142	42.25	0.652	5.565	0.569	8.28	0.272
		0.173	46.5	0.638	5.15	0.527	7.09	0.388
		0.179	47.6	0.633	4.815	0.493	6.52	0.520
		0.111	35.15	0.670	5.673	0.580	9.85	0.296
		0.104	33.65	0.673	5.69	0.582	10.27	0.299
		0.080	28.0		5.66	0.579	12.065	
		0.045	16.86		5.35	0.547	18.45	
		0.037	13.08		4.825	0.493	21.30	
II-1	75	0.028	7.0		3.19	0.326	26.11	
		0.035	12.04		4.29	0.439	20.58	
		0.048	18.1	0.582	5.07	0.518	16.31	0.244
		0.059	21.95	0.599	5.415	0.554	14.50	0.160
		0.063	23.2	0.604	5.43	0.555	13.79	0.173
		0.071	25.5	0.612	5.40	0.552	12.54	0.208

Table B.2 (Continued). Data of Impulsive Moment Coefficient C_δ

Run No.	Protrusion h/D (%)	p (inch)	Φ (degree)	C_I	M_F/r (gram)	C_F	W (gram)	C_δ
II-1	75	0.084	29.0	0.617	5.46	0.558	11.27	0.205
		0.106	34.0	0.633	5.49	0.561	9.82	0.246
		0.035	12.03		4.44	0.454	21.30	
		0.040	14.65		4.67	0.477	18.45	
		0.075	26.6	0.616	5.41	0.553	12.065	0.222
		0.087	29.65	0.624	5.22	0.533	10.55	0.249
		0.190	49.3	0.631	4.95	0.506	6.52	0.379
		0.179	47.6	0.635	5.19	0.530	7.03	0.431
		0.102	33.2	0.632	5.38	0.550	9.85	0.284
II-4	50	0.053	20.0	0.384	3.45	0.353	10.08	0.179
		0.095	31.55	0.430	3.70	0.378	7.07	0.265
		0.105	33.8	0.436	3.63	0.371	6.52	0.336
III-1	75	0.048	18.2		7.19	0.501	23.02	
		0.054	20.45		7.20	0.502	20.62	
		0.083	28.9		7.78	0.542	16.10	
		0.116	36.2	0.638	7.97	0.555	13.50	0.284
		0.169	45.9	0.640	7.94	0.553	11.06	0.290
		0.216	53.3	0.627	7.52	0.524	9.38	0.351
		0.271	61.2	0.600	7.10	0.494	8.11	0.368
		0.043	16.46		6.03	0.420	21.30	
		0.064	23.6		7.40	0.516	18.45	
		0.137	40.2	0.641	7.78	0.542	12.065	0.342
		0.164	45.0	0.640	7.45	0.519	10.55	0.431
		0.182	48.0	0.637	7.62	0.531	10.27	0.364
		0.182	48.0	0.637	7.33	0.510	9.855	0.454
		0.187	48.8	0.636	7.41	0.516	9.85	0.423
		0.307	66.05	0.576	6.46	0.450	7.07	0.583
		0.321	67.9	0.566	6.03	0.420	6.52	0.575

† Values of C_I are obtained from solid-line curves shown in Figures 6 and 7.

‡ $C_F = (M_F/r)/\zeta K$; K = 24.35 grams; ζ = 1.0 for all tests of Run I
K = 9.78 grams; ζ = 1.0 for all tests of Run II
K = 18.22 grams; ζ = 0.787 for Run III-1.

Table B.3. Pattern of Fluid-Dynamic Forces and Moments

at Protrusion Condition h/D = 100% (Run I-8)

i	p_i (inch)	Φ_i (degree)	$\sin \Phi_i$	$\cos \Phi_i$	$a_i = \frac{\cos \Phi_i}{-\cos \Phi_0}$	$b_i = \frac{\sin \Phi_i}{-\sin \Phi_0}$	$C_{Ii} = C_{Ri}$	$c_i = \frac{C_{Ii}}{-C_{I0}}$
0	0.190	49.3	0.758	0.652	-	-	0.781	-
1	0.238	56.5	0.833	0.551	-0.101	0.077	0.740	-0.041
2	0.331	69.2	0.935	0.3555	-0.2965	0.177	0.649	-0.132

$$C_D^* = (c_1 b_2 - c_2 b_1)/(a_1 b_2 - a_2 b_1) = 0.592$$

$$C_L^* = (a_1 c_2 - a_2 c_1)/(a_1 b_2 - a_2 b_1) = 0.232$$

$$\Phi_M = \arctan (C_L^*/C_D^*) = 21.4 \text{ degree}$$

$$C_C^* = C_{I0} - C_L^* \sin \Phi_0 - C_D^* \cos \Phi_0 = 0.219$$

$$C_{IM} = C_C^* + C_L^* \sin \Phi_M + C_D^* \cos \Phi_M = 0.854$$

Φ (degree)	$\cos \Phi$	$\sin \Phi$	$C_D^* \cos \Phi$	$C_L^* \sin \Phi$	$C_I^\dagger$
5	0.996	0.087	0.590	0.020	0.829
10	0.985	0.174	0.583	0.040	0.842
20	0.940	0.342	0.556	0.079	0.854
30	0.866	0.500	0.513	0.116	0.848
40	0.766	0.643	0.453	0.149	0.821
50	0.643	0.766	0.380	0.178	0.777
60	0.500	0.866	0.296	0.201	0.716
70	0.342	0.940	0.202	0.218	0.639
80	0.174	0.985	0.103	0.228	0.550

$^\dagger C_I = C_C^* + C_L^* \sin \Phi + C_D^* \cos \Phi$

Table B.4. Pattern of Fluid-Dynamic Forces and Moments at Protrusion Condition h/D = 85% (Run I-7)

i	p_i (inch)	Φ_i (degree)	sin Φ_i	cos Φ_i	$a_i = \frac{\cos \Phi_i}{-\cos \Phi_0}$	$b_i = \frac{\sin \Phi_i}{-\sin \Phi_0}$	$C_{Ii} = C_{Ri}$	$c_i = \frac{C_{Ii}}{-C_{I0}}$
0	0.107	34.27	0.563	0.826	-	-	0.671	-
1	0.172	46.40	0.724	0.690	-0.136	0.161	0.638	-0.033
2	0.329	68.94	0.933	0.360	-0.466	0.370	0.518	-0.153

$$C_D^* = (c_1 b_2 - c_2 b_1)/(a_1 b_2 - a_2 b_1) = 0.502$$

$$C_L^* = (a_1 c_2 - a_2 c_1)/(a_1 b_2 - a_2 b_1) = 0.219$$

$$\Phi_M = \arctan (C_L^*/C_D^*) = 23.6 \text{ degree}$$

$$C_C^* = C_{I0} - C_L^* \sin \Phi_0 - C_D^* \cos \Phi_0 = 0.133$$

$$C_{IM} = C_C^* + C_L^* \sin \Phi_M + C_D^* \cos \Phi_M = 0.680$$

Φ (degree)	cos Φ	sin Φ	C_D^* cos Φ	C_L^* sin Φ	C_I
5	0.996	0.087	0.500	0.019	0.652
10	0.985	0.174	0.494	0.038	0.665
20	0.940	0.342	0.472	0.075	0.680
30	0.866	0.500	0.435	0.110	0.678
40	0.766	0.643	0.384	0.141	0.658
50	0.643	0.766	0.323	0.168	0.624
60	0.500	0.866	0.251	0.190	0.574
70	0.342	0.940	0.172	0.206	0.511
80	0.174	0.985	0.087	0.216	0.436

Table B.5. Pattern of Fluid-Dynamic Forces and Moments

at Protrusion Condition h/D = 75% (Run I-9)

i	p_i (inch)	Φ_i (degree)	$\sin \Phi_i$	$\cos \Phi_i$	$a_i = \frac{\cos \Phi_i}{-\cos \Phi_0}$	$b_i = \frac{\sin \Phi_i}{-\sin \Phi_0}$	$C_{Ii} = C_{Ri}$	$c_i = \frac{C_{Ii}}{-C_{I0}}$
0	0.095	31.6	0.523	0.852	-	-	0.629	-
1	0.174	46.75	0.728	0.686	-0.166	0.205	0.633	0.007
2	0.314	67.0	0.921	0.391	-0.461	0.398	0.570	-0.059

$$C_D^* = (c_1 b_2 - c_2 b_1)/(a_1 b_2 - a_2 b_1) = 0.523$$

$$C_L^* = (a_1 c_2 - a_2 c_1)/(a_1 b_2 - a_2 b_1) = 0.457$$

$$\Phi_M = \arctan (C_L^*/C_D^*) = 41.1 \text{ degree}$$

$$C_C^* = C_{I0} - C_L^* \sin \Phi_0 - C_D^* \cos \Phi_0 = -0.056$$

$$C_{IM} = C_C^* + C_L^* \sin \Phi_M - C_D^* \cos \Phi_M = 0.638$$

Φ	$\cos \Phi$	$\sin \Phi$	$C_D^* \cos \Phi$	$C_L^* \sin \Phi$	C_I
5	0.996	0.087	0.521	0.040	0.505
10	0.985	0.174	0.516	0.080	0.540
20	0.940	0.342	0.492	0.156	0.592
30	0.866	0.500	0.453	0.228	0.625
40	0.766	0.643	0.401	0.294	0.638
50	0.643	0.766	0.337	0.350	0.631
60	0.500	0.866	0.262	0.396	0.602
70	0.342	0.940	0.179	0.429	0.552
80	0.174	0.985	0.091	0.450	0.485

Table B. 6. Pattern of Fluid-Dynamic Forces and Moments

at Protrusion Condition h/D = 50% (Run I-4)

i	p_i (inch)	Φ_i (degree)	$\sin \Phi_i$	$\cos \Phi_i$	$a_i = \cos \Phi_i - \cos \Phi_0$	$b_i = \sin \Phi_i - \sin \Phi_0$	$C_{Ii} = C_{Ri}$	$c_i = C_{Ii} - C_{I0}$
0	0.066	24.1	0.408	0.913	-	-	0.404	-
1	0.115	35.92	0.587	0.810	-0.103	0.179	0.443	0.039
2	0.246	57.73	0.845	0.534	-0.379	0.437	0.466	0.062

$$C_D^* = (c_1 b_2 - c_2 b_1)/(a_1 b_2 - a_2 b_1) = 0.258$$

$$C_L^* = (a_1 c_2 - a_2 c_1)/(a_1 b_2 - a_2 b_1) = 0.367$$

$$\Phi_M = \arctan (C_L^*/C_D^*) = 54.9 \text{ degree}$$

$$C_C^* = C_{I0} - C_L^* \sin \Phi_0 - C_D^* \cos \Phi_0 = 0.018$$

$$C_{IM} = C_C^* + C_L \sin \Phi_M + C_D \cos \Phi_M = 0.466$$

Φ (degree)	$\cos \Phi$	$\sin \Phi$	$C_D^* \cos \Phi$	$C_L^* \sin \Phi$	C_I
5	0.996	0.087	0.257	0.032	0.307
10	0.985	0.174	0.254	0.064	0.336
20	0.940	0.342	0.242	0.125	0.385
30	0.866	0.500	0.224	0.183	0.425
40	0.766	0.643	0.198	0.236	0.452
50	0.643	0.766	0.166	0.281	0.465
60	0.500	0.866	0.129	0.318	0.465
70	0.342	0.940	0.088	0.345	0.451
80	0.174	0.985	0.045	0.362	0.425

Table B.7. Pattern of Fluid-Dynamic Forces and Moments at Protrusion Condition h/D = 25% (Run I-5)

i	p_i (inch)	Φ_i (degree)	$\sin \Phi_i$	$\cos \Phi_i$	$a_i = \cos \Phi_i - \cos \Phi_0$	$b_i = \sin \Phi_i - \sin \Phi_0$	$C_{Ii} = C_{Ri}$	$c_i = C_{Ii} - C_{I0}$
0	0.034	11.48	0.199	0.980	-	-	0.191	-
1	0.095	31.6	0.524	0.852	-0.128	0.325	0.244	0.053
2	0.140	40.75	0.653	0.758	-0.222	0.454	0.259	0.068

$$C_D^* = (c_1 b_2 - c_2 b_1)/(a_1 b_2 - a_2 b_1) = 0.143$$

$$C_L^* = (a_1 c_2 - a_2 c_1)/(a_1 b_2 - a_2 b_1) = 0.222$$

$$\Phi_M = \arctan (C_L^*/C_D^*) = 57.2 \text{ degree}$$

$$C_C^* = C_{I0}^* - C_L^* \sin \Phi_0 - C_D^* \cos \Phi_0 = 0.007$$

$$C_{IM} = C_C^* + C_L^* \sin \Phi_M + C_D^* \cos \Phi_M = 0.270$$

Φ (degree)	$\cos \Phi$	$\sin \Phi$	$C_D^* \cos \Phi$	$C_L^* \sin \Phi$	C_I
5	0.996	0.087	0.143	0.019	0.169
10	0.985	0.174	0.141	0.040	0.187
20	0.940	0.342	0.134	0.076	0.217
30	0.866	0.500	0.124	0.111	0.242
40	0.766	0.643	0.110	0.143	0.260
50	0.643	0.766	0.092	0.170	0.269
60	0.500	0.866	0.072	0.191	0.270
70	0.342	0.940	0.049	0.209	0.265
80	0.174	0.985	0.025	0.219	0.251

LITERATURE CITED

(1) Albertson, M. L., Barton, J. R., and Simmons, D. B., "Fluid Mechanics for Engineers," Prentice-Hall Inc., Englewood Cliffs, New Jersey, (1960), p. 399.

(2) Allen, J., "Scale Models in Hydraulic Engineering," Longmans, Green and Co., London, pp. 407, (1947).

(3) Apperley, L. W., "The Effect of Turbulence on Sediment Entrainment," Ph.D. Thesis, School of Engineering, Univ. of Auckland, pp. 188 (Jan. 1968).

(4) Behera, Bhubaneshwar and Qureshy, Asrar Ahmad, "A Length Criterion for the Hydraulic Jump," M. S. Thesis, State University of Iowa, Iowa City, Iowa, pp. 53 (Feb. 1947).

(5) Carstens, M. R., Neilson, F. M., and Altinbilek, H. D., "Bed Forms Generated in the Laboratory under an Oscillatory Flow: Analytical and Experimental Study," Tech. Memorandum No. 28, U. S. Army Coastal Engineering Research Center, 105 pp. (June 1969).

(6) Chao, J. L. and Sandborn, V. A., "Study of Static Pressure along a Rough Boundary," Journal of Hydraulics Division, ASCE Proc. Paper 4269, pp. 193-204 (Mar. 1965).

(7) Cheng, E. D. H., "Incipient Motion of Large Roughness Elements in Open Channel Flow," Ph.D. Dissertation in Civil Eng., Utah State Univ., Logan, Utah, pp. 179 (1969).

(8) Chepil, W. S., "Equilibrium of Soil Grains at the Threshold of Movement by Wind," Soil Science Society Proceedings, Vol. 23, pp. 422-428 (1959).

(9) Einstein, H. A., "The Bed-Load Function for Sediment Transportation in Open Channel Flows," Technical Bulletin No. 1026 U. S. Dept. of Agriculture, Washington, D. C. (1950).

(10) Einstein, H. A., and El-Samni, El-Sayed Ahmed, "Hydrodynamic Forces on a Rough Wall," Reviews of Modern Physics, Vol. 21, No. 3, pp. 520-524 (July 1949).

(11) Gessler, J., "The Beginning of Bedload Movement of Mixtures investigated as Natural Armoring in Channels," (1965).
Translated by E. A. Prych
Translation T-5, W. M. Keck Laboratory of Hydraulics and Water Resources, California Inst. of Tech., Pasadena, Calif. (Revised Oct. 1968).

(12) Goncharov, V. N., "Dynamics of Channel Flow," (1962).
Translated from Russian by Israel Program for Scientific Translations, Jerusalem (1964), OTS 64-11003, 317 pp.

(13) Grass, A. J., "Initial Instability of Fine Bed Sand," Journal of the Hyd. Div., Proc. ASCE, HY3, Paper No. 7139, pp. 619-632 (Mar. 1970).

(14) Ippen, A. T. and Verma, R. P., "The Motion of Discrete Particles along the Bed of a Turbulent Stream," Proceedings, Minnesota IAHR Convention, pp. 7-20 (1953).

(15) Iwagaki, Y. and Tsuchiya, Y., "An Analysis of the Stable Cross Section of a Stream Channel," Disaster Prevention Research Institute Bulletin No. 29, March 1959, 27 pp.

(16) Jacob, W., "Strömung hinter einem einzelnen Rauhigkeitselement," Ingenieur-Archiv, IX, Band, pp. 343-355 (1938).

(17) Jacobsen, L. S., and Ayre, R. S., "Engineering Vibration," McGraw-Hill, New York, pp. 7-8 (1958).

(18) Jeffreys, H. J., "On the Transport of Sediments by Streams," Proceedings Cambridge Philosophical Society, Vol. 25, pp. 272-276, (1929).

(19) Kalinske, A. A., "Movement of Sediment as Bed Load in Rivers," Trans. American Geophysical Union, Vol. 28, No. 4, pp. 615-620, (August 1947).

(20) Klemin, A., Schaefer, E. B., and Beerer, J. G., "Aerodynamics of the Perisphere and Trylon at World's Fair," Transactions ASCE, pp. 1449-1468, (1939).

(21) Mavis, F. T. and Laushey, L. M., "A Reappraisal of the Beginning of Bed Movement Competent Velocity," Proc. IAHSR, Appendix 12, pp. 213-218, Stockholm, Sweden (1948).

(22) Naib, S. K. A., "Equilibrium of Talus Blocks Downstream of Stilling Basins," Water Power, London, pp. 407-410 (Oct. 1967).

(23) Neill, C. R., "Mean Velocity Criterion for Scour of Coarse Uniform Bed-Material," Paper C6, IAHR Congress Proceedings XII, Vol. 3, Fort Collins, Colorado, pp. 46-54 (1967).
"Note on Initial Movement of Coarse Uniform Bed-Material," Journal of Hydraulic Research, 6 (1968) No. 2, pp. 173-176.

(24) Novak, P., "Experimental and Theoretical Investigation of the Stability of Prisms on the Bottom of a Flume," Proceedings of Second IAHR Conference, Stockholm, Sweden, pp. 77-91 (1948).

(25) O'Brien, M. P., and Morison, J. R., "The Forces Exerted by Waves on Objects," Transactions of the American Geophysical Union, Vol. 33, No. 1, pp. 32-38 (Feb. 1952).

(26) Prandtl, L., "Essentials of Fluid Dynamics," English Translation, (1952), pp. 334-336.

(27) Rouse, H., "Elementary Mechanics of Fluids," John Wiley and Sons, (1946), pp. 191-196.

(28) Shields, A., "Anwendung der Aehnlichkeitsmechanik und der Turbulenz-forschung auf die Geschiebebewegung," Mitteilung der Preussischen Versuchsanstalt für Wasserbau und Schiffbau, Heft 26, Berlin (1936), "Applications of Similarity Principles and Turbulence Research to Bed-Load Movement," translated to English by W. P. Ott and J. C. van Uchelen, California Inst. of Tech., Pasadena, Calif., on file in the United Engineering Society Library.

(29) Thompson, S. M., "The Transport of Gravel by Rivers," Proceedings of the Second Australasian Conference on Hydraulics and Fluid Mechanics, pp. A259-A274, D16-D17 (Dec. 1965).

(30) Tieleman, H. W. and Sandborn, V. A., "A Three Dimensional Single Roughness Element in a Turbulent Boundary Layer," Prepared for U. S. Army Research Grant DA-AMC-28-043-64-G-9, AD623902, (Sept. 1965).

(31) Vanoni, V. A., "Sediment Transportation Mechanics: Initiation of Motion," Journal of the Hydraulic Division, ASCE, Vol. 92, No. HY2, Proc. Paper 4738, pp. 291-314 (Mar. 1966); Discussions and Closure.

(32) White, C. M., "The Equilibrium of Grains on the Bed of a Stream," Proc. Roy. Soc. (A) 174, No. 958 (1940).

(33) Young, D. F., "Drag and Lift on Spheres Within Cylindrical Tubes," Trans. ASCE, Vol. 126, Part I, Paper No. 3231, pp. 1235-1248 (1961).

VITA

Charng-ning Chen was born in Fu-Kien, China on August 25, 1939. He attended local public schools and graduated from Chien-Kuo High School, Taipei, Taiwan, China in June of 1957. He was graduated from Cheng-Kung University, Tainan, Taiwan, China, with a B.S. degree in Hydraulic Engineering in June 1961. After one year military service, he came to the United States to pursue graduate study at the State University of Iowa, Iowa City, Iowa, in September 1962. He was a research assistant of the Iowa Institute of Hydraulic Research during the academic year of 1962-1963. He was awarded a M.S. degree in Mechanics and Hydraulics from the University of Iowa in February 1964.

He was employed by the Board of Water Supply of New York City as an assistant civil engineer from December 1963 to December 1964. He worked for Burns and Roe, Inc., New York City, from December 1964 to July 1965, on the hydraulic designs of circulating water systems for thermal power plants. From July 1965 to August 1966, he was employed by Parsons, Brinkerhoff, Quade, and Douglas, Inc., New York City, on various assignments in the field of engineering hydraulics, soil dynamics, and sanitary engineering. In June of 1966, he attended a summer Institute of Water Pollution Control, Manhattan College, New York City, sponsored by the P.B.Q. & D. Inc. From September 1966 to September 1967 and during the summer of 1968, he has worked for Tippetts-Abbett-McCarthy-Strantton, Engineers and Architects, New York City, on various assignments of hydroelectric

projects and water resources developments. Excluding the summer of 1968, he attended the Graduate Division of the Georgia Institute of Technology from September 1967 to the present. He was a graduate research assistant of the School of Civil Engineering at the Georgia Institute of Technology.

He is an associate member of the American Society of Civil Engineers.

He is single.